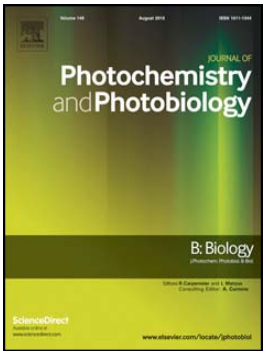

Synthesis, photophysical properties and systematic evaluations of new phenanthroimidazole fluorescent probe for bioimaging: Experimental and theoretical study

Przemysław Krawczyk, Beata Jedrzejewska, Marek Pietrzak, Tomasz Janek

PII: S1011-1344(16)30602-9
DOI: doi:10.1016/j.jphotobiol.2016.11.008
Reference: JPB 10649

To appear in:

Received date: 25 July 2016
Revised date: 22 September 2016
Accepted date: 5 November 2016

Please cite this article as: Przemysław Krawczyk, Beata Jedrzejewska, Marek Pietrzak, Tomasz Janek, Synthesis, photophysical properties and systematic evaluations of new phenanthroimidazole fluorescent probe for bioimaging: Experimental and theoretical study, (2016), doi:10.1016/j.jphotobiol.2016.11.008

Synthesis, photophysical properties and systematic evaluations of new phenanthroimidazole fluorescent probe for bioimaging: experimental and theoretical study

Przemysław Krawczyk[1*], Beata Jędrzejewska[2], Marek Pietrzak[2], Tomasz Janek[3]

[1] Nicolaus Copernicus University, Collegium Medicum, Faculty of Pharmacy, Department of Physical Chemistry, Kurpińskiego 5, 85-950 Bydgoszcz, Poland

[2] UTP University of Science and Technology, Faculty of Chemical Technology and Engineering, Seminaryjna 3, 85-326 Bydgoszcz, Poland

[3] Wroclaw Medical University, Department of Inorganic Chemistry, Faculty of Pharmacy, Borowska 211a, 50-556 Wroclaw, Poland

*Corresponding author: przemekk@cm.umk.pl; tel: +48 52 5853679

Abstract

In this study, the newly synthesized 4'-(1*H*-phenantro[9,10-d]-imidazol-2-yl)-bifenyl-4-carboaldehyde - PB2 was investigated as a fluorescent dye. For this reason, the spectroscopic properties in solvents of different polarity were studied. The experimental data were supported by quantum-chemical calculations using density functional theory. Measurements and theoretical calculations showed that PB2 compound is characterized by the non-monotonic solvatochromism, strongly polar charge transfer excited state, large Stokes' shift, high fluorescence quantum yield and high fluorescence lifetime. Simulations using AutoDock presented in this study, showed that after conjugation with Concanavalin A in the active site with LYS200, the PB2 possesses the highest probability of binding affinity. Circular

dichroism (CD) measurement was performed to monitor the changes of the secondary structure of Concanavalin A induced by the presence of PB2 fluorophore. These results indicate that the addition of PB2 influences the secondary structure of Concanavalin A, but does not affect the interactions with carbohydrate moieties. Finally, by using fluorescence microscopy it was demonstrated that the PB2 is the photostable fluorescent probe and PB2 conjugate Concanavalin A exhibits a blue fluorescence. The results of this study have implications in designing PB2-protein conjugate as a valuable alternative to commercial probes designed for cellular labeling in biological and biomedical research.

Keywords

Fluorochrome; Solvatochromism; Conjugation and Bioimaging; Electronic excited state; Density functional theory; AutoDock

1. Introduction

In recent years, one of the most developing branches of medical sciences is the fluorescence technology. This method allows for sensitive and easy study of intermolecular interactions and the transcriptional dynamics of the cell nucleus [1-2]. In particular, fluorescent imaging and flow cytometry become the standard and highly sensitive methods for detection of pathogens and their reliable location inside the human body [3-8]. In this field, *in vivo* the fluorescent imaging in medicinal diagnostics is the visualization technique of fluorescent probes pointing to the structural changes in tissues and biochemical processes. This allows for a detailed analysis and monitoring of the location and dynamics of genes, proteins, dyes expression and molecular interactions in cells, functionality of cells and physiological parameters in a less time-consuming way [9-10]. The signal from the fluorescent probe in site of interactions can be modulated and for this reason sensors relying on activation and not just accumulation, can be utilized. Nevertheless, one of the major steps in this science is to design and synthesize probes with the appropriate properties and thus this technology is often limited. Primarily, the fluorescent dyes used herein should have appropriate sensitivity and allow for the correct identification and quantitative determination by non-destructive and non-invasive analysis of biochemical processes *in vivo* at the cellular and molecular level [11-17]. Specific qualities are desirable for fluorescent nanostructures: low toxicity and good solubility, high chemical and environmental stability, tolerance by living cells and large penetration depth in living tissues, high photostability, large signal to noise ratio, sharp absorption and emission under excitation, large Stokes' shift, bright fluorescence, high quantum yield and resistance to photobleaching [18-21]. Furthermore, they require an appropriate and specific reactive group allowing for an easy connection to macromolecules. The most important ones are: -CHO, -NH_2, -SH, N-hydroxysuccinimide ester and isothiocyjanate groups.

The main aim of this study was the synthesis and spectroscopic characteristics of a new compound belonging to the imidazole class, containing -CHO as a functional group: 4'-(1*H*-phenantro[9,10-d]-imidazol-2-yl)-bifenyl-4-carboaldehyde - PB2. Imidazoles are very popular in many areas of clinical medicine and are widely used as: antiepileptic agents, antiparasitic, anthelmintic, anti-inflammatory, analgesics and platelet aggregation inhibitors [22-27], antineoplastic antibiotic, muscarinic receptor antagonist, antiulcerative, prohormone, benzodiazepine antagonist, antihyperthyroid and hypnotic agents [28-31], as well as ratiometric fluorescent probe for hydrogen sulfite [32], a ratiometric fluorescent probe for cysteine and hemocysteine [33], antimicrobial drug [34], sensitive fluorescence ratiometric probe for cyanide with its application for detection of cyanide in natural water samples and biological samples [35], solar cells [36], multifunctional agents for treatment of Alzheimer's disease [37]. Therefore, the primary objective of this work was to evaluate the usefulness of the newly synthesized PB2 dye in potential applications as fluorescent probes in living cell imaging technology and flow cytometry. The experimental data were supported by quantum-chemical calculations using density functional theory (DFT) [38-44]. The choice of this method is due to its adequate precision in reproducing experimental data, from structural to spectroscopic parameters of many classes of compounds at relatively low computational costs [45-54]. The theoretical investigations were supplemented by molecular docking in exploring the best binding site, to which the PB2 has the highest affinity.

2. Methodology section

2.1. Experimental part

2.1.1. Materials and synthesis

All reagents and solvents were obtained from Aldrich Chemical Co. The 2-(4-bromophenyl)-phenanthro[9,10-d]imidazole was synthesized based on the procedures taken from literature [55].

The 4'-(1*H*-phenanthro[9,10-d]-imidazol-2-yl)-biphenyl-4-carboaldehyde, PB2 was obtained according to literature [56] using 2-(4-bromophenyl)-phenanthro[9,10-d]imidazole (2,7 mmol), 4-formylphenylboronic acid (3 mmol), $P(Ph_3)Pd(OAc)_2$ (0,011 mmol), 1-propanol (15-20 mL), Na_2CO_{3aq} (6 mL, 2M), water (5 mL + 20 mL) and 2% $NaHCO_3$ [Fig 1].

Fig.1.

$C_{28}H_{18}N_2O$; 398.45532 g/mol; mp 267.5 ^oC; 36.9% yield; R_f = 0.36 for methanol-chloroform 0.1:10 v/v.

^1H NMR (DMSO-d_6) δ (ppm): 7.67 (m, 2H, Ar), 7.77 (m, 2H, Ar), 8.06 (m, 6H, Ar), 8.48-8.46 (d, *J*=8.0 Hz, 2H, Ar), 8.60-8.58 (d, *J*=8.0 Hz, 1H, Ar), 8.64-8.62 (d, *J*=8.0 Hz, 1H, Ar), 8.87-8.85 (d, 1H, *J*=8.0 Hz, Ar), 8.91-8.89 (d, *J*=8.0 Hz, 1H, Ar), 10.09 (s, 1H, C*H*O), 13.58 (s, 1H, N*H*)

^{13}C NMR (DMSO-d_6) δ (ppm): 193.2 (*C*HO), 122.4, 122.5, 124.3, 124.6, 125.7, 126.0, 127.2, 127.6, 127.7, 127.8, 128.1, 130.7 (*C*H), 122.8, 127.4, 128.3, 128.4, 130.9, 135.7, 137.7, 139.6, 145.4, 148.9 (*C*)

IR (KBr) (cm^{-1}): 3604, 3048, 1699, 1601, 1559, 1530, 1481, 1455, 1429, 1308, 1269, 1221, 1169, 1044, 1003, 961, 820, 761, 746, 725, 691, 614, 499

Throughout the manuscript the following notation was adopted: 1.4-Dx - 1.4-dioxane; Et_2O - diethyl ether; THF - tetrahydrofuran; MeCN - acetonitrile; DMF - N,N-DiMethylFormamide; DMSO - DiMethylSulfoxide.

2.1.2. Measurements

The ^{1}H (400 MHz) and ^{13}C (100 MHz) NMR spectra were recorded on a Bruker Ascend^{TM} 400 NMR spectrometers. Dimethylsulfoxide (DMSO-d_6) was used as the solvent and tetramethylsilane (TMS) as internal standard.

The IR spectra of the synthesized salts were recorded using a Bruker Vector 22 FT-IR spectrophotometer (Germany) in the range 400-4500 cm^{-1}, by KBr pellet technique.

HPLC analysis was done by Waters HPLC systems equipped with Waters 2489 UV-Vis detector (detection wavelength was 370 nm), Waters 1525 Binary HPLC Pump and a Symmetry C18 column (3.5 μm, 4.6 × 75 mm). Separation was conducted under isocratic conditions with 0.8 ml/min flow rate, 25°C, 10 μl injection volume and HPLC grade acetonitrile as a mobile phase.

Melting points were determined on the Buchi M-565 Melting Point apparatus.

Absorption and emission spectra in solvents of different polarity were recorded at room temperature using a Shimadzu UV-vis Multispec-1501 spectrophotometer and a Hitachi F-4500 spectrofluorimeter, respectively.

The fluorescence quantum yield of the tested compounds (ϕ) was calculated using equation (1):

$$\phi = \phi_{ref} \frac{IA_{ref}}{I_{ref}A} \cdot \frac{n^2}{n_{ref}^2} \quad (1)$$

where:

ϕ_{ref} is the fluorescence quantum yield of the reference (Coumarin 1 in ethanol ϕ_{ref} = 0.64 [57]) sample in ethanol, A and A_{ref} are the absorbencies of the compound under study and reference sample at the excitation wavelength (404 nm), I and I_{ref} are the integrated emission

intensities for the tested compounds and reference sample, n and n_{ref} are the refractive indexes of the solvents used for the compounds and the reference, respectively.

The fluorescence lifetimes were measured using an Edinburgh Instruments single-photon counting system (FLS920P Spectrometers). The excitation was provided by a picosecond diode laser generating pulses of about 55 ps at 375 nm. The compounds were studied at a concentration needed to provide absorbance of 0.2-0.3 in a 10 mm cell at 375 nm. The fluorescence decays were fitted as sums of two exponentials. The average lifetime, τ_{av} was calculated as $\tau_{av} = (\Sigma_i \alpha_i \tau_i)/(\Sigma_i \alpha_i)$, where α_i and τ_i are the amplitudes and lifetimes.

2.1.3. General protein labeling procedures

Concanavalin A (carbohydrate-binding protein) was conjugated with a PB2-fluorophore in phosphate-buffered saline (PBS, 10mM phosphate, 150mM NaCl, pH 7.4). Briefly, two milligram of Concanavalin A was resuspended in 1 mL of buffer solution and 50 µL of 5 mg/mL PB2 in dimethyl sulfoxide (DMSO) was added during vigorous mixing. The Schiff bases formed by amine-aldehyde coupling were reduced by adding 10 µL of 5M sodium cyanoborohydride in 1 N NaOH per 1 mL reaction volume, and the reaction was allowed to proceed overnight at 4 °C. After an overnight incubation at 4 °C in the dark, unlabeled PB2 dyes were separated using a dialysis membrane centrifuge tube at 7000*g* for 10 min. The conjugated PB2-Concanavalin A solution retained in the dialysis tube was collected and diluted in PBS to a protein concentration of 1 mg/mL. The degree of labeling was determined by measuring the absorbance at 280 nm for Concanavalin A and at λ_{ABS} of the PB2 on a Varian Carry 50 Bio spectrophotometer (Varian, USA). The resultant product was stored at 4 °C.

2.1.4. Fluorescence imaging

Candida albicans ATCC 10231 and *Yarrowia lipolytica* A101 strains were grown in a liquid yeast-peptone-glucose (YPG) medium consisting of (per liter) 10 g of yeast extract, 20

g of peptone (both from Difco), and 20 g of glucose at 28 °C with constant shaking at 200 rpm. The overnight cultures of both yeast strains were centrifuged and washed twice with PBS, pH 7.4. Then, the yeast cells were stained for 30 min at 28 °C with PB2-Concanavalin A conjugate (final concentration 0.025 mg/mL) in the PBS. Images were obtained using a Zeiss Axio Scope A1 microscope (Zeiss, Jena, Germany) with a 100× objective lens and Zeiss filter set FS01 for fluorescence microscopy. Assays were carried out three times. Representative images are presented in Fig. 5.

2.1.5. Circular dichroism spectroscopy

Circular dichroism spectra of 0.1 mg/mL Concanavalin A solutions were recorded on a Jasco model J-1500 spectropolarimeter (Jasco, Tokyo, Japan) at 25 °C under a constant flow of nitrogen gas, in the absence and presence of a PB2 probe. The scanned wavelength domain was 190–260 nm and the time constant, scan speed, bandwidth/resolution, 50 nm/min, 2 nm and 200 millidegrees, respectively. The spectra represent the average of 9 scans. CD intensities are expressed in $\Delta\varepsilon$ ($dm^3 \cdot mol^{-1} \cdot cm^{-1}$). The analysis of secondary structural contents was performed using K2D3 web server. K2D3 web server is an online tool used to assess the secondary structural elements in the form of α-helix and β-strand from the far-UV CD spectra ranging from 190 to 240 nm [58].

2.2. Computational details

The geometrical parameters of PB1 dye in its ground (S_g) and excited (S_{CT}) state were optimized by using density functional theory (DFT) approach, with the PBE0 functional [59-60] implemented in Gaussian 09 program package [61] with TIGHT threshold option. Inclusion of this functional to designate the molecular structures is justified by the correct description of the spectroscopic parameters in terms of experimental data for many classes of D-π-A dyes [62-64]. For each optimized structure of the ground and excited state, the analysis

of Hessians was conducted to verify that all the structures correspond to the minima on the potential energy surface.

By applying the time-dependent density functional theory (TDDFT) [46-48] vertical absorption and emission spectra were determined. The TDDFT treats the S_g and S_{CT} states with equilibrium solvation. For the best consideration of the solvent impact on the fluorescence spectra, the ground state should be calculated with non-equilibrium solvation [65-66]. This was taken into account by including the state-specific (SS) corrected linear response (cLR) approach [67] to the theoretical calculations. In the SS approach the solvent dynamic polarizations are determined by the difference of the electron densities of the initial and final states [68-70].

The polarity of the excited state was evaluated by numerical differentiation of the excitation energies (*E*):

$$\Delta\mu_{ge}^{i} = \frac{E_{CT}\left(+F^{i}\right)-E_{CT}\left(-F^{i}\right)}{-2F^{i}} - \frac{E_{g}\left(+F^{i}\right)-E_{g}\left(-F^{i}\right)}{-2F^{i}} \qquad (2)$$

where *i* states for the Cartesian component of the dipole moment difference. In these calculations there was used an electric field *F* of 0.001 a.u. strength.

Calculations of the spectroscopic parameters were conducted in connection with standard-hybrid PBE0 functional, as well as long-range asymptotically corrected LC-ωPBE [71-73], CAM-B3LYP [74] and ωB97XD [75] functionals. The solvent effect on the linear optical properties has been taken into account using the Integral Equation Formalism for the Polarisable Continuum Model (IEF–PCM) [76-77].

The AutoDock 4.2 [78-80] simulations were applied to identify the site with the highest affinity of PB2 dye relative to protein. The explorations of the binding site were performed using a united-atom scoring function implemented in AutoDock Vina [81]. The AutoDock Tools software package was used in order to prepare the PB2 molecule as a ligand and Concanavalin A as a macromolecule. All the water molecules and Ca, Mg and Xe atoms

were removed from the crystal structure of Concanavalin-A downloaded from the Protein Data Bank in Europe (PDB ID: 2a7a) [82]. According to the literature [83], the conjugation of molecules containing aldehyde as a functional group with a macromolecule occurs via formation of a Shift base between the aldehyde and an amino group of a lysine residue. Then, a reduction to a secondary or tertiary amine occurs, which gives a stable alkylamine bond. In order to reflect this, the grid box was adjusted in such way that the space included the individual -NH2 group of lysine's side chain, in subsequent simulations. The docking region on the target protein was defined by establishing a grid box with the dimensions of X: 18; Y: 18; Z: 18 Å, with a grid spacing of 1 Å. In AutoDock 4.2 simulations, the Lamarkian genetic algorithm was employed to identify appropriate binding energy and conformation of the PB1 dye. For each atom of the receptor molecule, Gasteiger charges were calculated. The docking procedure was repeated ten times for each lysine.

The simulations of biological activity were performed using a combination of the 3D/4D QSAR BiS/MC and CoCon algorithms developed by ChemoSophia company [84-86].

3. Results and discussion

3.1. Experimental

3.1.1. Absorption and fluorescence spectra

Figure 1 shows the illustrative electronic absorption and the fluorescence spectra for the tested compound in selected solvents. Table 1 collects the values of the absorption and fluorescence maximum positions, molar absorption coefficients, Stokes shifts and fluorescence quantum yields for the phenanthroimidazole derivative. Their electronic absorption spectra displays a broad band with a maximum in the range from 370.5 to 377.5 nm and high molar absorption coefficients ranging from 35 900 $M^{-1}cm^{-1}$ to 44 600 $M^{-1}cm^{-1}$. The inspection of the data in Table 1 shows that the position of the π-π^* absorption band

depends slightly on solvent polarity. This indicates a less polar character of the compounds in the ground state.

Table 1.

Fig. 2.

As indicated in Figure 2 and Table 1, the solvent polarity significantly affects the position of fluorescence spectral maxima. The emission spectra are red-shifted by ca. 80 nm as the solvent polarity increases. This, exemplified by the increase of emission maximum from 465 nm in diethyl ether to 545 nm in DMSO, observably indicates the change in charge distribution within the molecules in the singlet excited state. Reasonable correlation has been found between both the fluorescence peak maxima and the Stokes' shift parameter and the solvent polarity scale, E_T^N (Fig.3).

The substantial red shift of the emission spectra and an increase of Stokes shift with solvent polarity suggest an increase of the dipole moment in the excited state with respect to that of the ground state.

Fig. 3.

Besides fluorescence band position also its intensity is affected by solvent polarity. As shown in Fig. 4, the fluorescence quantum yield of PB2 decreases with increasing solvent polarity E_T^N. Such behaviour is characteristic for compounds with a highly polar ICT excited state [87]. The decrease in fluorescence intensity with increasing solvent polarity indicates that the PB2 reveals a positive solvatokinetic behaviour. According to literature data [88-90], in such a case a non-radiative decay is prominent in the compound due to efficient internal conversion and/or intersystem crossing by extensive mixing between the close-lying $^1(\pi\text{-}\pi^*)$ and $^1(\text{n-}\pi^*)$ states. The observed linear correlation between the fluorescence quantum yields of PB2 and E_T^N scale demonstrates the opposite effect to the previously studied compound PB1 (4-(1*H*-phenanthro[9,10-d]-imidazol-2-yl)-benzaldehyde) [91]. This means that introduction

of the second phenyl ring to the structure of the PB1 affects the fluorescence properties to a great extent.

Fig. 4.

For the tested compound two-exponential fluorescence decays were observed (Table 2), with first components lifetime close to 2 ns and the second of about 0.3-0.6 ns. Moreover, the shortest average fluorescence lifetimes are observed in diethyl ether. The correlation between the fluorescence average lifetimes and E_T^N solvent polarity parameter for PB2 clearly demonstrates the sensitivity of its fluorescence behaviour to the solvents. The fluorescence lifetimes increase with an increase of solvent polarity. What is more, for PB2 the fluorescence quantum yield is indirectly proportional to its lifetime i.e. as the ϕ_{Fl} decreases with increase of solvent polarity, the τ_{Fl} increases. This is probably due to the strong interaction between the strongly polarized molecule and solvents in the excited state.

Table 2.

Based on the average lifetimes and quantum yields of fluorescence data, radiative (k_r) and nonradiative (k_{nr}) rate constants have been calculated according to Eqs. 3 and 4. The values are collected in Table 3.

$$k_r = \frac{\phi_{Fl}}{\tau_{av}} \tag{3}$$

$$k_{nr} = \frac{(1-\phi_{Fl})}{\tau_{av}} \tag{4}$$

Analysis of the data collected in Table 3 indicates that the k_r/k_{nr} ratio changes with solvent polarity. For PB2 compound the ratio increases with increasing polarity of the medium pointing to the increasing role of non-radiative processes, due to the enhancement of intersystem crossing, internal conversion and vibrational deactivation [92-94]

Table 3.

The obtained spectral results suggest that PB2 may be available for use as a fluorescence labeling reagent for the circular dichroism measurements and fluorescence microscopy of glycoproteins in biological samples.

3.1.2. Protein labeling with PB2 fluorophore

The binding of the probes to protein has gained importance in a lot of different fields in biomedical research. This method is based on the fluorescence detection of macromolecules (such as proteins or antibodies) labeled with probes [95-96]. The PB2 probes with reactive aldehyde groups formed Schiff bases with the primary amines of Concanavalin A. The reaction efficiency and bond stability between aldehydes and primary amines was increased by the addition of sodium cyanoborohydride.

The internalization of the synthesized probe was examined at cellular level of the *Candida albicans* and *Yarrowia lipolytica* cells using fluorescence microscopy to achieve the optimal concentration and time exposition. The spectral study shows that the PB2-Concanavalin A conjugates accumulated selectively in yeast cells exhibits a blue fluorescence with excitation filter BP 365/12 nm and LP 397 nm emission filter (Fig. 5). On the basis of our results, it is concluded that the PB2-Concanavalin A conjugate is characterized by strong and stable fluorescence, what is a promising sign for serious application for this compound as a fluorophore for biomolecules. Our data were compared to those obtained performing a similar systematic study on the interaction of fluorescein isothiocyanate (FITC), one of the most used fluorescent probes for labeling of proteins and antibodies [97-98]. Our results recommend PB2 as a possible valuable alternative to FITC for use as fluorescent label for proteins. Our further studies will include the labeling of antibodies, by taking advantage of the reactive group on PB2 (−CHO) able to bind covalently to amines, lysine ε-amines and N-terminal α-amines groups of the antibody, and studying the antigen–antibody interaction.

Fig. 5.

3.1.3. Effects of PB2 on the Concanavalin A secondary structure

The circular dichroism spectrum of Concanavalin A is that of a typical lectin, with a negative band near 220 nm revealing a content of β-sheet structure [99]. Fitting the spectrum of native Concanavalin A at 25 °C yielded a 40.04% β-sheet and only 2.97% α-helical structure. The PB2-Concanavalin A conjugate caused a secondary structural change of the lectin to 26.55% β-sheet/14.22% α-helical. These spectral changes suggest the occurrence of bulk conformational modifications due to fluorophore binding to the primary amines of Concanavalin A (Fig. 6).

Fig. 6.

3.2. Theoretical aspect

For the investigated dye, the lowest-lying singlet excited state is the CT state (bright state). Structures and geometrical parameters of the PB2 dye after optimization were shown in Fig. 7 and Table S1. Firstly, the CT state is more planar than the ground state. The S_g is twisted on C8-C10 bond and during excitation this twisting is not observed. For S_{CT} dihedral angles 7-8-10-11 and 9-8-10-15 become smaller by more than 2.2° while 7-8-10-15 and 9-8-10-11 angles become larger by more than 2.2°. After the excitation, the twisting on the C13-C16, which is present in S_g and S_{CT}, undergoes a slight straightening. In this case, for the ground state dihedral angles 12-13-16-17 and 14-13-16-21 are longer by 22° and 12-13-16-21 and 14-13-16-17 are shorter by more than 22°. Although in the CT state bonds linking aromatic parts (C8-C10, C13-C16, C19-C22) are reduced by more than 0.025Å, the structure of the excited state seems to be longer (C1/2-C22). This is due to the fact that aromatic rings are slightly flattened and bonds such as N7-C8 and N9-C8 are lengthened by over 0.017. Not without significance is the effect of solvent on the structure of the tested dye. Primarily, the structure of ground state is shortened while for the S_{CT} it is lengthened in the function of the solvent polarity. Mainly, this is the result of reduction of the dihedral angles for S_g and increasing

them for S_{CT}. Moreover, for both structures there can be discerned a linear increase or decrease of the bond lengths and angles relative to the polarity of the environment. The exception is water where this relation is often disrupted. This observation is in correlation with the solubility of the PB1 molecule, in relation to the free energy of solvation ($\Delta G_{solvation}$) [100] (see Table 4). In water the $\Delta G_{solvation}$ adopts the smallest value, decreased by more than 45% relative to the MeCN for which it has the greatest value. This growth in conjunction with structural changes significantly affects the solubility in water. The PB2 dyes is very weakly soluble in water and the calculated solubility is: $5.4 \cdot 10^{-7}$ mol/l (in 25°C, 298.15 K, 760 mmHg).

Fig. 7.

Table 4.

According to Fig. 8, the charge transfer excitation is dominated by HOMO-LUMO transition. The HOMO is distributed over the entire molecule while the LUMO is mainly located on the benzaldehyde fragment and partially on the imidazole part. The -CHO group is a moderately deactivating substituent but after excitation the electron-cloud mainly accumulates on benzaldehyde. For this reason, the lowest-lying excited state can be assigned as a π-π* transition mixed with ICT process. In this system, the C8-Ar-C22 plays the role of the system with π-conjugated double bonds and may be favourable for nonlinear optical properties. Moreover, in all solvents the studied dye is characterized by high value of the E_{GAP} (over 3 eV, see Table S2) which indicates a high fluorescent efficiency and good stability [93]. The value of chemical hardness (η), predicted from HOMO-LUMO, is relatively low and therefore the PB2 should be treated as a soft molecule. For this reason, its reactivity is very high and it undergoes uni-molecular reaction (such as with proteins) relatively quickly and easily.

Fig. 8.

Fig. 9.

Fig. 9 presents the molecular electrostatic potential (MEP). The MEP analysis is very useful in designing new fluorescent probes because localizing the active electrophilic and nucleophilic region specifies the sites where the molecule can participate in the formation of H-bonds as well as determines the intermolecular interaction. The PB2 dye has two strong regions for electrophilic attack (red sites) localized on C20 and at the C14-C15 bond. Thus, the extensions of the molecule by the introduction of an additional benzene ring relative to the 4-(1*H*-phenanthro[9,10-d]-imidazol-2-yl)-benzaldehyde (PB1) [91] causes a constant negative site at C12 (benzaldehyde part) and the appearance of an additional region in the middle ring. In addition, the external imidazole rings adopt a more negative value than in the case of PB1. Maximum positive (blue) sites for nucleophilic reactivity are localized on the hydrogen atom at the N7-H. However, in contrast to PB1 where only one strong positive region was observed, in the case of PB2 dye strongly positive electrostatic sites also appear at the C13-C16 bond linking the benzene rings and in the central imidazole ring. Thus, increasing the structure of the molecule is associated with increasing the potential sites from where the dye can experience intermolecular as well as can undergo non-covalent interactions.

Table 5.

Theoretically determined one-photon absorption spectra (λ_{calc}^{Ab}, OPA) are listed in Tables 5 and S3. Among the vertical excitation energies (ΔE), the values closest to experimental ones are obtained using PBE0 functional. Its application shifts the maximum of the λ_{calc}^{Ab} towards longer wavelengths, however this bathochromic shift is not large and on average is 27 nm. In turn, the long-corrected functionals lead to significantly overestimated ΔE and the average error is 36 nm, 62.6 nm and 46 nm for CAM-B3LYP, LC-ωPBE and ωB97XD, respectively. As mentioned earlier, in the absorption process the ground state should be considered in non-equilibrium solvation and therefore the cLR-TDDFT calculations

have been performed (see Table S4). Firstly, the cLR approach gives the OPA maxima shifted towards longer wavelengths and the values obtained for the long-corrected functionals are approaching the experimental data. In the case of PBE0, including the state-specific solvation correction causes that the error for PBE0 becomes larger and the overestimation is on average 47.6 nm. This time, the functional giving the most reliable results turned out to be ωB97XD, which induces a bathochromic shift by only 14 nm. Such correct predictions for this functional were not observed in the case of PB1 dye. What is more important, both models in an analogous way describe the solvatochromic behaviour. Presented data shows, that PB2 dye is characterized by non-monotonic solvatochromism. The transition from gas phase to the weakly polar solvent is associated with the red shift and for theoretical data it occurs up to THF. In a more polar MeCN the opposite is visible but in DMF there is a positive solvatochromism. In DMSO there are some inconsistencies, because in terms of solvatochromic behaviour the results consistent with the measured values are obtained with TDDFT, while cLR-TDDFT provides a hypsochromic shift. In water, for both approaches there is observed a re-negative solvatochromism. The PB1 dye was characterized by the same solvatochromic behaviour. Taking into account the measured data, placing an additional benzene ring in the structure of the PB2 dye results in a shift of the maximum absorption bands in the direction of longer wavelengths by only 1 nm in weakly polar and 4 nm in polar solvents. For TDDFT calculations these values are 1nm and 3nm but for cLR-TDDFT they increase to 12nm and 6 nm, respectively.

According to HOMO-LUMO plots, photoexcitation to the charge-transfer state leads to substantial changes in the electron density of the solute and these differences in the solute-solvent electrostatic interaction energy between S_g and S_{CT} induce a strong solvatochromic shift. For this reason, a linear dependence of the solvatochromic shift on the dipole moment difference ($\Delta\mu_{g-CT}$) between ground (μ_g) and CT states (μ_{CT}) should be excepted. For

compounds with positive solvatochromism, $\mu_{CT} > \mu_g$ and the excited state is characterized by a high polarity which results in a significant decrease of the ΔE. In contrast, the blue shift occurs when the ground state is better stabilized by polar solvents than the CT state and $\mu_g > \mu_{CT}$ what intensifies the ΔE of the solute. Moreover, the hypsochromic shift occurs also when H-bond interactions are present which additionally enhances the intensity of the CT absorption band [102]. For the tested PB2 dye, a $\mu_{CT} > \mu_g$ dependency is observed in all solvents (see Table S5). Dipole moments of the ground and CT states increase in the function of solvent polarity, except for DMF where μ_{CT} is reduced by about 0.1D. The PB2 exhibits strongly polar charge-transfer state ($\Delta\mu_{g-CT}$ > than 13 D and 8 D for PBE0 and CAM-B3LYP respectively) but this uptrend cannot be concluded explicitly. For PBE0, the $\Delta\mu_{g-CT}$ enhances with the solvent polarity and only in DMF a disorder of this behaviour is observed. For other functionals, the increase of $\Delta\mu_{g-CT}$ follows up to Et_2O while from THF it is reduced and only in water there is observed an enhancement of the CT state polarity. For this reason, the pure electrostatic contributions to the solvent-solute interactions do not occur and the short-range specific interactions such as H-bond or self-aggregation should be expected. The comparison of the vertical OPA determined theoretically and experimentally (see Fig.10) also reveals some inconsistencies. In the region of interest, an additional peak in the measured absorption spectra is visible in the main band, near 350nm. For TDDFT this peak is more separated and located at 310 nm. However, in all cases this peak as well as the main band have the same intensity and occur independently of the solvent polarity. Therefore, the reasons for its formation should be sought in a n-π^* transition or the presence of the aldehyde group (additionally calculated maxima of the λ_{calc}^{Ab} are: benzaldehyde - 195.17 nm; acetaldehyde - 206.73 and 245.50 nm; formaldehyde - 223.70 nm, see Fig. S1). In this connection it should be assumed that PB2 dye, as well as PB1, tend to self-aggregate in medium and polar environments which induces the reversal solvatochromism [103-104]. This is in accordance

with the MEP plots where there are regions from which the studied compound can undergo not only H-bond interactions with protein but also with other molecules. As it can be derived from previously presented research [64] this situation does not have a significant effect on the in-vivo studies.

Fig. 10.

The calculated emission spectra (λ_{calc}^{Fl}) were shown in Tables 5 and S6. As in the case of the OPA spectra, closest to the experimental data are λ_{calc}^{Fl} obtained using PBE0. This functional overestimates the de-excitation energy in weakly polar 1,4-Dx and Et_2O and underestimates it in polar MeCN, DMF and DMSO. In each case $\Delta\lambda_{Exp-PBE0}^{Fl}$> 12 nm. The asymptotically corrected functionals shifted λ_{calc}^{Fl} towards shorter wavelengths by more than 30 nm and among them the values closer to measured ones are given by CAM-B3LYP. In THF the used functionals provide the fluorescence maximum with an error at the lowest level, while for MeCN and DMSO discrepancies are the highest in relation to the experimental data. After state-specific correction, PBE0 shifts the bands maxima in the direction of longer wavelengths and as a result increases the difference to the measured values. For other functionals, the SS correction does not work correctly. After using cLR-TDDFT, the differences in λ_{calc}^{Fl} between computed and measured values are significantly increased and the hypschromic effect is enhanced. On the other hand, predictability of solvatochromic behvior is similar in both approaches. Transition from the vacuum to weakly polar 1,4-Dx is associated with a bathochromic shift. From Et2O the non-monotonic behavior in function of the solvent polarity is observed. The reversal solvatochromism visible in Et_2O and in polar solvents confirms the conclusions for the OPA about solute-solvent interactions. Moreover, similarly to the λ_{calc}^{Abs}, the electric permittivity of the environment does not affect the intensity of the fluorescence spectra and the additional peak disappears. These observations do not allow to clearly exclude the possibility of H-bonds formation. However, they confirmed that

in less polar solvents the PB2 dye tends mainly to self-aggregate, while in strongly polar ones the specific solute-solvent interactions may occur. Similar conclusions came from the analysis of the PB1 dye.

One of the coefficients specifying the usefulness of a dye as a fluorescent probe in bioimaging is the Stokes' shift. As mentioned in experimental part, the PB2 is characterized by a large value of $\Delta\nu^{St}$ which increases as a function of solvent polarity but is slightly decreased in water. For *ab inito* calculations, only PBE0 effectively reflects the behavior of Stokes' shift in relation to the solvent. For asymptotically corrected functionals a decline in the $\Delta\nu^{St}$ value occurs from MeCN while in water these values grow. In the case of PBE0, the Stokes' shift increases with increasing dielectric constant up to water, where it is reduced. However, the values nearest to the experimental ones are obtained with CAM-B3LYP and $\Delta\nu^{St}$ is underestimated, except for water, and the average relative error is 147.6 cm^{-1}. For PBE0 the average overestimation is 1881.6 cm^{-1}. The use of state-specific approach leads to underestimation of the $\Delta\nu^{St}$ which enhances the difference to the measured data. Despite the fact that both functionals correctly reproduce the behaviour of the Stokes' shift relative to the solvent, the $\Delta\Delta^{St}_{Exp-cLR-TDDFT}$ are 6338.2 cm^{-1} and 2098.9 cm^{-1} for CAM-B3LYP and PBE0 respectively. Analogous dependence was observed for the PB1 dye. Therefore it should be noted that PBE0 is almost a universal tool in the description of spectroscopic properties of fluorescent probes.

As mentioned in the methodology section, the conjugation of PB2 with Conacavalin A occurs via formation of a Shift base between the aldehyde of the dye and amino groups of a lysine residue and next by reduction (with participation of $NaBH_4$ which acts as the reductive agent) to a secondary or tertiary amine to give a stable alkylamine bond. Thus, it is possible to connect the dye to a macromolecule in several places. In order to identify the most probable site for dye-protein conjugation, the AutoDock procedure was employed. As shown in Table

S7, the lowest binding free energy (ΔG_b in kcal/mol) characterizes the sites with LYS200 and the calculated inhibition constant (K_i) is 0.24 mM. In this active site, the PB2 dye posses the highest probability of potential binding affinity with the active site of the Concanavalin A [105-106]. As it was shown in Fig. 11, in this location the fluorochrome probe is efficiently inserted into the aromatic cage formed by LYS200 and GLY45 interacts with aldehyde group; SER201 directed toward C16 and SER164 interacting with imidazole part. This binding is not stabilized by the π-π stacking interaction and also the presence of H-bonds is not observed. The slightly higher value of ΔG_b is observed for the binding active site created by the VAL79, ILE29, LYS30 and ASN237, where LYS30 is directed towards C11 in central ring. However, the $\Delta\Delta G_b$ between these locations is only 0.2 kcal/mol and the K_i value is doubled and increases to 0.45 mM. As before, a π-π stacking interaction is not observed, as well as no H-bonds. For the third binding active site (LYS114) with a relatively high affinity, the ΔG_b increases to -5.4 kcal/mol and K_i is increased to 0.70 mM. The PB2 is sandwiched between the aromatic cage of LYS14, THR123, THR112, HIS127, GLU192 and MET129. The fluorochrome is positioned by CHO group towards THR123 and LYS114 interacts with C16 of benzaldehyde. Moreover, in this location a H-bond forms between N7-H and the oxygen atom of the THR112 (3.125 Å) which is consistent with the MEP analysis. The formation of a H-bond may have an effect on the growth of the inhibition constant. For the active site with LYS101 with lower affinity and where H-bond is not observed, the K_i is reduced by 0.29 mM. In all active binding sites the PB2 dye is twisted with respect to the reference geometry (S_g). This twisting occurs on the C8-C10 and C13-C16 bonds. The biggest twisting is observed in the location with LYS200 where the torsion angle C8-C10-C16-O23 changes form -34.2° for the S_g structure to 69.4° after docking. Additionally, the O23 in the aldehyde group is oriented in a line with N7-H hydrogen. For other mentioned binding modes this angle is decreased and the oxygen atom remains in the orientation analogous to S_g.

Fig. 11.

Requirements for fluorescent probes are not only the specific characteristics of their spectroscopic properties, but also specific physicochemical features. One of them is the bioavailability [107]. The possibility and rate of penetration through biological membranes and consequently, probability of achieving an appropriate concentration in the region of action is referred to LogP. This value determines the absorption and the permeability across cell membranes. For the PB2 dye the calculated LogP = 4,85 ±0.36 and according to the Lipinski "5" rule, is characterized by relatively good bioavailability [108]. The studied compound is characterized by high metabolism at CYP-450 (the calculated probabilities are 0.6668 and 0.9938 for the CYP450-2D6 and CYP450-3A4, respectively). So, after completing the task as a fluorescent marker, it will be quickly removed from the body without interacting with other drugs [109]. Another important parameter indicating bioconcentration is LogBCF. It refers to the process of uptake and build up of chemicals in living organisms. The calculated LogBCF = --4.89558 and suggests that PB2 molecule will not be bioaccumulative in living organisms. Moreover, the calculated probability of toxicity is 0.46 ±0.1 what indicates a moderate toxicity (the range 0.2-08). Therefore, insertion of an additional benzene ring relative to the PB2 dye does not amend significant difference to LogP ($\Delta LogP_{PB2\text{-}PB1}$ = 0.04) and LogBCF ($\Delta LogBCF_{PB2\text{-}PB1}$ = 1.01). However, it reduces the probability of toxicity by 0.23. On the other hand, the PB2 can be used in many other areas of medical sciences. This dye is characterized by many biological activities and exhibits such properties as: Anti-Tumor Cycline-dependent kinase 4 inhibitory activity; Anti-Tumor DNA anti-metabolitic activity; HIV1-proteaze inhibitory activity and others (see Fig.S2).

Conclusions

Synthesis, spectral, photophysical and some of biological activities in different solvents of new phenanthroimidazole derivatives: 4'-(1*H*-phenantro[9,10-d]-imidazol-2-yl)-bifenyl-4-carboaldehyde (PB2) were presented. The experimental measurements showed a significant effect on the position of absorption and emission spectra. The emission spectra are red-shifted by ca. 80 nm resulting in a large Stokes' shift. The high molar absorption coefficient, indicating intramolecular charge transfer (ICT) characteristics of the transition and decreasing the fluorescence quantum yield in function of solvent polarity, suggests that PB2 is characterized by a highly polar ICT excited state. For this dye, the fluorescence quantum yield is indirectly proportional to the lifetime which may be due to some interaction between the strongly polarized molecule and solvents in the excited state. The theoretical calculated vertical excitation energies, as well as the state-specific corrected linear response approach clearly indicate that PB2 compound exhibits the non-monotonic solvatochromism. By contrast, the correlations of the polarity of the CT state in function of solvent polarity showed that this dye exhibits strongly polar charge transfer excited state and a red shift should occur. Therefore, the observed non-monotonic behaviour is associated with a tendency of self-aggregation in some environments which also may affect the solubility. The AutoDock simulations pointed out that the active site near LYS200 is the most probable location where the conjugation of PB2 with Conconavalin A will occur. This binding active site is characterized by lowest ΔG_b values and the inhibition constant is only 0.24 mM. Interactions with macromolecules are purely van der Waals interactions and no π-π stacking nor H-bonds are observed. Moreover, theoretical calculations showed that CT state is more planar than the ground state and after docking the structure of PB2 dye undergoes greater twisting, which occurs on the C8-C10 and C13-C16 bonds. The usefulness of this compound in biomedical imaging was confirmed by fluorescence microscopy imaging. The *in-vitro* study showed that

the PB2 conjugate Concanavalin A exhibited a blue fluorescence with high stability and intensity. Therefore this compound has potential applicability as a fluorescent probe for protein detection, for example for labelling of lectins, for detection of specific carbohydrate moieties and antibodies for immunofluorescence assays. On the other hand, the tested dye is characterized by moderate toxicity, good bioavailability and low bioaccumulative in living organisms. All of these properties make the PB2 dye a promising potential compound for fluorescence bioimaging.

Acknowledgements

This research was supported by the Computational Grant No. 249, PCSS (Poznan, Poland); in part by PL-Grid Infrastructure; BS 9/2014. *Yarrowia lipolytica* A101 was a kind gift of Dr. Aleksandra Mirończuk (Department of Biotechnology and Food Microbiology, Wrocław University of Environmental and Life Sciences, Wroclaw, Poland).

Supporting Information Available: Analytical data, molecular structure and spectroscopic properties for investigated compound.

Submission declaration

Submitting the article " Synthesis, photophysical properties and systematic evaluations of new phenanthroimidazole fluorescent probe for bioimaging: experimental and theoretical study" to The Journal of Photochemistry and Photobiology B: Biology has not been published previously, is not under consideration for publication elsewhere, publication is approved by all authors and it will not be published elsewhere including electronically in the same form, in English or in any other language, without the written consent of the copyright-holder.

Conflict of interest

The authors declare that there are no conflicts of interest.

Declaration of interest

Submitting the article "Synthesis, photophysical properties and systematic evaluations of new phenanthroimidazole fluorescent probe for bioimaging: experimental and theoretical study" to The Journal of Photochemistry and Photobiology B: Biology does not have any potential conflicts of financial and non-financial interests.

References:

[1] P. Mitra, M. Banerjee, S. Biswas, S. Basu, Protein interactions of Merocyanine 540: spectroscopic and crystallographic studies with lysozyme as a model protein, J. Photochem. Photobiol. B 121 (2013) 46-56, DOI: 10.1016/j.jphotobiol.2013.02.010.

[2] N. Romanov, C. Anastasi, X. Liu, Cyanine dyes for labeling molecular ligands with improved fluorescence intensity and photostability, 2013: WO2013041117 A1.

[3] M. Fernández-Suárez, A.Y. Ting, Fluorescent probes for super-resolution imaging in living cells, Nat. Rev. Mol. Cell. Biol. 9 (2008) 929-943, DOI: 10.1038/nrm2531.

[4] C. Basford, N. Forraz, C. McGuckin, Optimized multiparametric immunophenotyping of umbilical cord blood cells by flow cytometry, Nat. Protoc. 5(7) (2010) 1337-1346. DOI: 10.1038/nprot.2010.88

[5] A. Tanimura, Development and application of fluorescent protein-based indicators for live cell imaging**,** J. Oral. Biosci. 57 (2015) 54 – 60, DOI: 10.1016/j.job.2015.02.006.

[6] X. Zhang, S. Li, Z. Liu, S. Wang, J. Xiao Self-assembled multicolor nanoparticles based on functionalized twistacene dendrimer for cell fluorescent imaging, NPG Asia Mater. 7 (2015) 230-10, DOI: 10.1038/am.2015.126.

[7] J. Liu, Y.Q. Sun, H. Zhang, H. Shi, Y. Shi, W. Guo, Sulfone-Rhodamines: A new class of near-infrared fluorescent dyes for bioimaging." ACS Appl. Mater. Interfaces. 8(35) (2016) 22953–22962, DOI: 10.1021/acsami.6b08338.

[8] Y.-J. Gong et al, A unique approach toward near-infrared fluorescent probes for bioimaging with remarkably enhanced contrast, Chemical Science 7 (2016) 2275-2285, **DOI:** 10.1039/C5SC04014K.

[9] S. Lindström, Flow cytometry and microscopy as means of studying single cells: a short introductional overview, Methods. Mol. Biol. 853 (2012) 13-15, DOI: 10.1007/978-1-61779-567-1_2.

[10] M. Díaz, M. Herrero, L.A. Garcia, C. Quirós, Application of flow cytometry to industrial microbial bioprocesses, Biochem. Eng. J. 48(3) (2010) 385-407, DOI: 10.1016/j.bej.2009.07.013.

[11] R. Weissleder, V. Pittet, Imaging in the era of molecular oncology, Nature 4522 (2008) 580-589, DOI: 10.1038/nature06917.

[12] L.E. Jennings, N.J. Long, 'Two is better than one'-probes for dual-modality molecular imaging, Chem. Commun. 24 (2009) 3511-3524, DOI: 10.1039/B821903F.

[13] J.-M. Liu, J.-T. Chen, X.-P. Yan, Near infrared fluorescent trypsin stabilized gold nanoclusters as surface plasmon enhanced energy transfer biosensor and in vivo cancer imaging bioprobe, Anal. Chem. 85 (2013) 3238-3245, DOI: 10.1021/ac303603f.

[14] H. Guo, N.M. Idris, Y. Zhang, LRET-based biodetection of DNA release in live cells using surface-modified upconverting fluorescent nanoparticles, Langmuir 27 (2011) 2854-2860, DOI: 10.1021/la102872v.

[15] Z. Li, Y. Zhang, S. Jiang, Multicolor core/shell-structured upconversion fluorescent nanoparticles, Adv. Mater. 20 (2008) 4765-4769, DOI: 10.1002/adma.200801056.

[16] F. Rijke, H. Zijlmans, S. Li, T. Vail, A.K. Raap, R.S. Niedbala, H.J. Tanke, Up-converting phosphor reporters for nucleic acid microarrays, Nat. Biotechnol. 19 (2001) 273-276. DOI: 10.1038/85734.

[17] J. Kim, H.S. Kim, N. Lee, T. Kim, H. Kim, T. Yu, I.C. Song, W.K. Moon, T. Hyeon, Multifunctional uniform nanoparticles composed of a magnetite nanocrystal core and a mesoporous silica shell for magnetic resonance and fluorescence imaging and for drug delivery, Angew. Chem. Int. Ed. Engl. 47(44) (2008) 8438-8441, DOI: 10.1002/anie.200802469.

[18] D. Janczewski, Y. Zhang, G.K. Das, D.K. Yi, P. Padmanabhan, K.K. Bhakoo, T.T. Tan, S.T. Selvan, Bimodal magnetic-fluorescent probes forbioimaging, Microsc. Res. Tech. 74 (2011) 563-576. DOI: 10.1002/jemt.20912.

[19] M. Tsuji, S. Ueda, T. Hirayama, K. Okuda, Y. Sakaguchi, A. Isono, H. Nagasawa, FRET-based imaging of transbilayer movement of pepducin in living cells by novel intracellular bioreductively activatable fluorescent probes, Org. Biomol. Chem. 11 (2013) 3030-3037, DOI: 10.1039/C3OB27445D.

[20] F. Auzel, Upconversion and anti-stokes processes with f and d ions in solids, Chem. Rev. 104 (2004) 139-174, DOI: 10.1021/cr020357g.

[21] A. Germond, H.Fujita, T. Ichimura, T.M. Watanabe, Design and development of genetically encoded fluorescent sensors to monitor intracellular chemical and physical parameters, Biophys. Rev. 8 (2) (2016) 121-138, DOI: 10.1007/s12551-016-0195-9.

[22] U. Uçucu, N.G. Karaburun, I. Işikdağ, Synthesis and analgesic activity of some 1-benzyl-2-substituted-4,5-diphenyl-1H-imidazole derivatives, Farmaco. 56 (2001) 285-290, DOI: 10.1016/S0014-827X(01)01076-X.

[23] A. Yeşilada, S. Koyunoğlu, N. Saygili, E. Kupeli, E. Yeşilada, E. Bedir, I. Khanc, Synthesis, anti-inflammatory and analgesic activity screening of some new 4-(3H)-quinazolinone derivatives, Arch. Pharm. Pharm. Med. Chem. 337 (2004) 96-104, DOI: 10.1002/ardp.200200752.

[24] L. Quattara, M. Debaert, R. Cavier, Synthesis and antiparasitic activity of new nitro-5-imidazole derivatives, Farmaco. (sci) 42(6) (1987) 449-456, PMID:2904887

[25] S. Dutta, Synthesis and anthelmintic activity of some novel 2-substituted-4,5-diphenyl imidazoles, Acta. Pharm. 60(2) (2010) 229-235. DOI: 10.2478/v10007-010-0011-1.

[26] A.K. Sengupta, T. Bhattacharya, Synthesis and antimicrobial activity of some substituted 2-phenyl-3-arylquinazol-4-ones, J. Indian. Chem. Soc. 60 (1983) 373-376, DOI: 10.1002/chin.198349246.

[27] L. Navidpour, H. Shadnia, H. Shafaroodi, M. Amini, R. Dehpour, A. Shafiee, Design, synthesis and biological evaluation of substituted 2-alkylthio-1,5-diarylimidazoles as selective COX-2 inhibitors, Bioorg. Med. Chem. 15 (2007) 1976-1982, DOI: 10.1016/j.bmc.2006.12.041.

[28] G. Fluoret, Synthesis of pyroglutamylhistidylprolineamide by classical and solid phase methods, J. Med. Chem. 13 (1970) 843-845, DOI: 10.1021/jm00299a011.

[29] R.N. Brogden, R.C. Heel, T.M. Speight, G.S. Avery, Metronidazole in anaerobic infections: A review of its activity, pharmacokinetics and therapeutic use, Drugs 16(5) (1978) 387-417, PMID:363399.

[30] R.W. Brimblecombe, W.A.M. Duncan, G.J. Durant, J.C. Emmett, C.R. Ganellin, M.E. Parsons, J.W. Black, The pharmacology of cimetidine, a new histamine H_2-receptor antagonist, Br. J. Pharmacol. 53 (1975) 435–436, DOI: 10.1111/j.1476-5381.2010.00854.x.

[31] W. Hunkeler, H. Möhler, L. Pieri, P. Polc, E.P. Bonetti, R. Cumin, R. Schaffner, W. Haefely, Selective antagonists of benzodiazepines, Nature 290 (1981) 514-516, DOI: 10.1038/290514a0.

[32] X. Cheng, H. Jia, J. Feng, J. Qin, Z. Li, "Reactive" probe for hydrogen sulfite: Good ratiometric response and bioimaging application, Sensors and Actuators B 184 (2013) 274-280, DOI: 10.1016/j.snb.2013.04.070.

[33] W. Lin, L. Long, L. Yuan, Z. Cao, B. Chen, W. Tan, A Ratiometric fluorescent probe for cysteine and homocysteine displaying a large emission shift, Org. Lett. 10(24) (2008) 5577-5580. DOI: 10.1021/ol802436j.

[34] Jawaharmal, H.S. Lamba, S. Narwal, G. Singh, D.R. Saini, A. Kaur, S. Narwal, Synthesis of novel imidazole compounds and evaluation of their antimicrobial activity, Indo. Global. J. Pharm. Sci. 2(2) (2012) 147-156, ISSN 2249-1023.

[35] L. Long, L. Zhou, L. Wang, S. Meng, A. Gong, F. Du, C. Zhang, A highly selective and sensitive fluorescence ratiometric probe for cyanide and its application for detection of cyanide in natural water sample and biological sample, Anal. Methods. 5 (2013) 6605-6610, DOI: 10.1039/C3AY41475B.

[36] M.-S. Tsai, Y.-C. Hsu, J.T. Lin, H.-C. Chen, C.-P. Hsu, Organic dyes containing 1H-phenanthro[9,10-d]imidazole conjugation for solar cells, J. Phys. Chem. C 111(50) (2007) 18785-18793, DOI: 10.1021/jp075653h.

[37] J. Liu, J. Qiu, M. Wang, L. Wang, L. Su, J. Gao, Q. Gua, J. Xu, S.L. Huang, L.Q. Gu, Z.S. Huang, D. Li, Synthesis and characterization of 1H-phenanthro[9,10-d]imidazole derivatives as multifunctional agents for treatment of Alzheimer's disease, Biochim. Biophys. Acta 1840(9) (2014) 2886-2903, DOI: 10.1016/j.bbagen.2014.05.005.

[38] P. Hohenberg, W. Kohn, Inhomogeneous electron gas, Phys. Rev. 136 (1964) B864-B871, DOI: 10.1103/physrev.136.b864.

[39] W. Kohn, L.J. Sham, Self-consistent equations including exchange and correlation effects, Phys. Rev. 140 (1965) A1133-A1138, DOI: 10.1103/physrev.140.a113.

[40] R.G. Parr,W. Yang, Density-functional theory of atoms and molecules, Oxford Univ. Press, Oxford, 1989.

[41] Ed.D.R. Salahub, M.C. Zerner, The challenge of d and f electrons, ACS, Washington DC, 1989.

[42] C. Sosa, C. Lee, Density-functional description of transition structures using nonlocal corrections. Silylene insertion reactions into the hydrogen molecule, J. Chem. Phys. 98 (1993) 8004-8011, DOI: 10.1063/1.464554.

[43] G.E. Scuseria, Comparison of coupled-cluster results with a hybrid of Hartree-Fock and density functional theory, J. Chem. Phys. 97 (1992) 7528-7530, DOI: 10.1063/1.463977.

[44] Ed.J.K. Labanowski, J.W. Andzelm, Density Functional Methods in Chemistry, Springer-Verlag, New York, 1991.

[45] M. Kurt, T.R. Sertbakan, M. Ozduran, An experimental and theoretical study of molecular structure and vibrational spectra of 3- and 4-pyridineboronic acid molecules by density functional theory calculations, Spectrochim. Acta Part A 70(3) (2008) 664-673, DOI: 10.1016/j.saa.2007.08.019

[46] C. Adamo, G.E. Scuseria, V. Barone, Accurate excitation energies from time-dependent density functional theory: Assessing the PBE0 model, J. Chem. Phys. 111 (1999) 2889-2899, DOI: 10.1063/1.479571.

[47] C.J. Jamorski-Jödicke, H.P. Lüthi, Time-dependent density-functional theory investigation of the formation of the charge transfer excited state for a series of aromatic donor–acceptor Part I, J. Chem. Phys. 117 (2002) 4146-4156, DOI: 10.1063/1.1498817.

[48] V. Cavillot, B. Champagne, Time-dependent density functional theory simulation of UV/visible absorption spectra of zirconocene catalysts, Chem. Phys. Lett. 354 (2002) 449-457, DOI: 10.1016/S0009-2614(02)00161-6.

[49] C. Ravikumar, I.H. Joe, V.S. Jayakumar, Charge transfer interactions and nonlinear optical properties of push–pull chromophore benzaldehyde phenylhydrazone: A vibrational approach, Chem. Phys. Lett. 460 (2008) 552–558, DOI: 10.1016/j.cplett.2008.06.047

[50] R. Zhang, B. Du, G. Sun, Y. Sun Y**,** Experimental and theoretical studies on o-, m- and p-chlorobenzylideneaminoantipyrines, Spectrochim. Acta Part A 75 (2010) 1115-1124, DOI: 10.1016/j.saa.2009.12.067.

[51] F.J.A. Ferrer, F. Santoro, R. Improta, The excited state behaviour of cytosine in the gas phase: A TD-DFT study, Comp. Theor. Chem. 1040-1041 (2014) 186-194, DOI: 10.1016/j.comptc.2014.03.010.

[52] N. Sekar, P.G. Umape, V.S. Padalkar, R.P. Tayade, P. Ramasami, Synthesis of novel styryl derivatives from 4-chloro-2-(morpholin-4-yl)-1,3-thiazole-5-carbaldehyde, study of their photophysical properties and DFT computations, J. Lumin. 150 (2014) 8-18, DOI: 10.1016/j.jlumin.2014.01.060.

[53] H. Wang et al, Synthesis and characteristics of novel fluorescence dyes based on chromeno[4,3,2-de][1,6]naphthyridine framework, Spectrochim. Acta Part A 103 (2013) 62-67, DOI: 10.1016/j.saa.2012.10.075.

[54] H. Wang at al, Spectral studies of multi-branched fluorescence dyes based on triphenylpyridine core, Spectrochim. Acta Part A 121 (2014) 121:355-362, DOI: 10.1016/j.saa.2013.10.087.

[55] R. Francke, R.D. Little, Optimizing electron transfer mediators based on arylimidazoles by ring fusion: synthesis, electrochemistry, and computational analysis of 2-aryl-1-methylphenanthro[9,10-*d*]imidazoles, J. Am. Chem. Soc. 136(1) (2014) 427-435, DOI: 10.1021/ja410865z.

[56] B. Jędrzejewska, M. Gordel, J. Szeremeta, P. Krawczyk, M. Samoć, Synthesis, linear and nonlinear optical properties of three push-pull oxazol-5-(4H)-one compounds, J. Org. Chem. 80 (2015) 9641-9651, DOI: 10.1021/acs.joc.5b01636.

[57] J. Olmsted III, Calorimetric determinations of absolute fluorescence quantum yields, J. Phys. Chem. 83(20) (1979) 2557-682, DOI: 10.1021/j100483a006.

[58] C. Louis-Jeune, M.A. Andrade-Navarro, C. Perez-Iratxeta, Prediction of protein secondary structure from circular dichroism using theoretically derived spectra, Proteins. 80(2) (2011) 374-81, DOI: 10.1002/prot.23188.

[59] J.P Perdew, K. Burke, M. Ernzerhof, Generalized gradient approximation made simple, Phys. Rev. Lett. 77 (1996) 3865-3868, DOI: 10.1103/PhysRevLett.77.3865.

[60] J.P. Perdew, K. Burke, M. Ernzerhof, Errata: Generalized gradient approximation made simple, Phys. Rev. Lett. 78 (1997) 1396. DOI: 10.1103/PhysRevLett.78.1396.

[61] M.J. Frisch, G.W. Trucks, G.B. Schlegel et al. Gaussian 09, Revision A.1, Gaussian, Inc., Wallingford CT, 2009.

[62] B. Jędrzejewska, P. Krawczyk, M. Gordel, M. Samoć, Synthesis and photophysical properties of two-photon chromophores containing 1H-benzimidazole residue, Dyes Pigm. 162 (2014) 162-175, DOI: 10.1016/j.dyepig.2014.06.007.

[63] P. Krawczyk, Time-dependent density functional theory calculations of the solvatochromism of some azo sulfonamide fluorochromes, J. Mol. Model. 21 (2015) 118-136, DOI: 10.1007/s00894-015-2651-z.

[64] P. Krawczyk, M. Pietrzak, T. Janek, B. Jędrzejewska, P. Cysewski, Spectroscopic and nonlinear optical properties of new chalcone fluorescent probes for bioimaging applications: theoretical and experimental study, J. Mol. Model. 22 (2016) 125-136, DOI: 10.1007/s00894-016-2990-4.

[65] N. Minezawa, State-specific solvation effect on the intramolecular charge transfer reaction in solution: A linear-response free energy TDDFT method, Chem. Phys. Lett. 608 (2014) 140-144, DOI: j.cplett.2014.05.104.

[66] G.S. Ming Tong, K.T. Chan, X. Chang, Ch.-M. Che, Theoretical studies on the photophysical properties of luminescent pincer gold(III) arylacetylide complexes: the role of p-conjugation at the C-deprotonated [C^N^C] ligand, Chem. Sci. 6 (2015) 3026-3037, DOI: 10.1039/c4sc03697b.

[67] C. Guido, S. Caprasecca, Corrected linear response. State-specific correction to solvent polarization response, https://www1.dcci.unipi.it/molecolab/tools/white-papers/pisalr/; 2016, DOI: 10.13140/RG.2.1.1903.7845.

[68] L.V. Slipchenko, Solvation of the excited states of chromophores in polarizable environment: orbital relaxation versus polarization, J. Phys. Chem. A 114 (2010) 8824-8830, DOI: 10.1021/jp101797a.

[69] K. Sneskov, T. Schwabe, O. Christiansen, J. Kongsted, Scrutinizing the effects of polarization in QM/MM excited state calculations, Phys. Chem. Chem. Phys. 13 (2011) 18551-18560, DOI: 10.1039/C1CP22067E.

[70] M. Caricato, A Comparison between state-specific and linear-response formalisms for the calculation of vertical electronic transition energy in solution with the CCSD-PCM method, J. Chem. Phys. 139 (2013) 044116-9. DOI: 10.1063/1.4816482.

[71] H. Iikura, T. Tsuneda, T. Yanai, K Hirao, Long-range correction scheme for generalized-gradient-approximation exchange functionals, J. Chem. Phys. 115 (2001) 3540-3544, DOI: 10.1063/1.1383587.

[72] O.A. Vydrov, G.E. Scuseria, Assessment of a long range corrected hybrid functional, J. Chem. Phys. 125 (2006) 234109-9, DOI: 10.1063/1.2409292.

[73] O.A. Vydrov, G.E. Scuseria, J.P. Perdew, Tests of functionals for systems with fractional electron number, J. Chem. Phys. 126 (2007) 1541009-9. DOI: 10.1063/1.2723119.

[74] T. Yanai, D.P. Tew, N.C. Handy, A new hybrid exchange-correlation functional using the Coulomb-attenuating method (CAM-B3LYP), Chem. Phys. Lett. 393 (2004) 51-57, DOI: 10.1016/j.cplett.2004.06.011.

[75] J.D. Chai, M. Head-Gordon, Long-range corrected hybrid density functionals with damped atom-atom dispersion corrections, Phys. Chem. Chem. Phys. 10 (2008) 6615-6620. DOI: 10.1039/B810189B.

[76] M.T. Cancés, B. Mennucci, J. Tomasi, A new integral equation formalism for the polarizable continuum model: Theoretical background and applications to isotropic and anisotropic dielectrics, J. Chem. Phys. 107 (1997) 3032-3041, DOI: 10.1063/1.474659.

[77] M. Arivazhagan, P. Muniappan, R. Meenakshi, G. Rajavel, PCM/TD-DFT analysis of 1-bromo-2,3-dichlorobenzene – A combined study of experimental (FT-IR and FT-Raman) and theoretical calculations, Spectrochim. Acta Part A 105 (2013) 497-508, DOI: 10.1016/j.saa.2012.11.033.

[78] G.M. Morris, R. Huey, W. Lindstrom, M.F. Sanner, R.K. Belew, D.S. Goodsell, A.J. Olson, Autodock4 and AutoDockTools4: automated docking with selective receptor flexibility, J. Comput. Chem. 30 (2009) 2785-2791, DOI: 10.1002/jcc.21256.

[79] S. Cosconati, S. Forli, A.L. Perryman, R. Harris, D.S. Goodsell, A.J. Olson, Virtual screening with AutoDock: theory and practice, Expert Opin. Drug Discovery 5 (2010) 597-607, DOI: 10.1517/17460441.2010.484460.

[80] S. Forli, A.J. Olson, A force field with discrete displaceable waters and desolvations entropy for hydrated ligand docking, J. Med. Chem. 55 (2012) 623-638, DOI: 10.1021/jm2005145.

[81] O. Trott, A.J. Olson, AutoDock Vina: improving the speed and accuracy of docking with a new scoring function, efficient optimization and multithreading, J. Comp. Chem. 31 (2010) 455-461, DOI: 10.1002/jcc.21334.

[82] C. Mueller-Dieckmann, S. Panjikar, P.A. Tucker, M.S. Weiss**,** On the routine use of soft X-rays in macromolecular crystallography. Part III. The optimal data-collection wavelength, Acta Crystallogr. D Biol. Crystallogr. 61 (2005) 1263-1272, DOI: 10.2210/pdb2a7e/pdb.

[83] N. Jentof, D.G. Dearborn, Labeling of proteins by reductive methylation using sodium cyanoborohydride, J. Biol. Chem. 254(11) (1979) 4359-4365, PMID:571437.

[84] V. Potemkin, M. Grishina, Principles for 3D/4D QSAR classification of drugs, Drug Discov. Today 13(21-22) (2008) 952-959, DOI: 10.1016/j.drudis.2008.07.006.

[85] V. Potemkin, M. Grishina, A new paradigm for pattern recognition of drugs, J. Comput. Aided. Mol. Des. 22(6-7) (2008) 489-505. DOI: 10.1007/s10822-008-9203-x.

[86] V.A. Potemkin, A.A. Pogrebnoy, M.A. Grishina, Technique for energy decomposition in the study of "receptor-ligand" complexes, J. Chem. Inf. Model. 49(6) (2009) 1389-406, DOI: 10.1021/ci800405n.

[87] B. Jędrzejewska, B. Ośmiałowski, R. Zaleśny, Application of spectroscopic and theoretical methods in the studies of photoisomerization and photophysical properties of the push –pull styryl-benzimidazole dyes, Photochem. Photobiol. Sci. 15 (2016) 117-128, DOI: 10.1039/c5pp00361j.

[88] S.A. El-Daly, A.M. Asiri, M.A. Hussein, A.G. Al-Sehemi, Spectroscopic and computational studies of 1,4-bis[b-(6-tertbutyl-2-benzoxazolyl)vinyl]benzene, J. Lumin. 148 (2014) 317–324, DOI: 10.1016/j.jlumin.2013.12.047.

[89] S.A. El-Daly, E.M. Ebeid EM, Spectroscopic studies, fluorescence quenching by molecular oxygen and amplifief spontaneous emission of 1,4-bis[2-(2-pyridyl)vinyl]benzene, J. Mol. Struct. 1063 (2014) 213-218, DOI: 10.1016/j.molstruc.2014.01.003.

[90] S.A. El-Daly, K.A. Alamry, Spectroscopic investigation and photophysics of a D-π-A-π-D type styryl pyrazine derivative, J. Fluoresc. 26 (2016) 163–176, DOI: 10.1007/s10895-015-1698-7.

[91] P. Krawczyk, B. Jędrzejewska, M. Pietrzak, T. Janek T, Synthesis, spectroscopic and physicochemical properties and binding site analysis of 4-(1*H*-phenanthro[9,10-d]-imidazol-2-yl)-benzaldehyde day for flow cytometry and living cell imaging: experimental and theoretical study. J. Photochem. Photobiol. B, In press, DOI: 10.1016/j.jphotobiol.2016.07.044.

[92] M. Shaikh, J. Mohanty, P.K. Singh, A.C. Bhasikuttan, R.N. Rajule, V.S. Satam, S.R. Bendre, V.R. Kanetkar, H. Pal, Contrasting solvent polarity effect on the photophysical properties of two newly synthesized aminostyryl dyes in the lower and in the higher solvent polarity regions, J. Phys. Chem. A 114 (2010) 4507-4519, DOI: 10.1021/jp9107969.

[93] T. Shim, M.H. Le, D. Kim, Y. Ouchi, Comparison of photophysical properties of the hemicyanine dyes in ionic and nonionic solvents, J. Phys. Chem. B 112(7) (2008) 1906-1912, DOI: 10.1021/jp076757v.

[94] S.A. El-Daly, A.M. Asiri, S.A. Khan, K.A. Alamry, Spectral properties and micellization of 1-(2,5-dimethyl-thiophene-3-yl)-3-(2,4,5-trimethoxy-phenyl)-propenone(DTTP) in different media, J. Lumin. 134 (2013) 819-824, DOI: 10.1016/j.jlumin.2012.06.043.

[95] M. Brinkley, A brief survey of methods for preparing protein conjugates with dyes, haptens, and cross-linking reagents, Bioconjug. Chem. 3(1) (1992) 2-13, DOI: 10.1021/bc00013a001.

[96] A. Holmberg, A. Blomstergren, O. Nord, M. Lukacs, J. Lundeberg, M. Uhlen, The biotin-streptavidin interaction can be reversibly broken using water at elevated temperatures, Electrophoresis. 26(3) (2005) 501-510, DOI: 10.1002/elps.200410070.

[97] G. Grunwaldt,S. Haebel, C. Spitz, M. Steup, R. Menzel, Multiple binding sites of fluorescein isothiocyanate moieties on myoglobin: photophysical heterogeneity as revealed by ground-and excited-state spectroscopy, J. Photochem. Photobiol. B 67 (2002) 177-186, DOI: 10.1016/S1011-1344(02)00323-8.

[98] D. Stan, C.-M. Mihailescu, M. Savin, I. Matei, 2-(2-Hydroxy-5-nitrobenzylidene)-1, 3-indanedione versus fluorescein isothiocyanate in interaction with Anti-hFABP immunoglobulin G1: Fluorescence quenching, secondary structure alteration and binding sites localization, *Int. J. Mol. Sci. 14*(2) (2013) 3011-3025, DOI:10.3390/ijms14023011.

[99] S.W. Provencher, J. Glockner, Estimation of globular protein secondary structure from circular dichroism, Biochemistry. 20(1) (1981) 33-37. DOI: 10.1021/bi00504a006.

[100] A. Kaczmarek-Kędziera, M Ziegler-Borowska, D. Kędziora, Chemia obliczeniowa w laboratorium organicznym, Wydawnictwo UMK, Toruń, 2014.

[101] R.V. Solomon, R. Jagadeesan, S.A. Vedha, P. Venuvanalingam, A DFT/TDDFT modeling of bithiophene azo chromophores for optoelectronic applications, Dyes Pigm. 100 (2014) 261-268, DOI: 10.1016/j.dyepig.2013.09.016.

[102] W. Bartkowiak, Solvatochromism and nonlinear optical properties of donor-acceptor π-conjugated molecules, In: M.G. Papadopoulos, A.J. Sadlej, J. Leszczynski, Non-linear optical properties of matter; from molecules to condensed phases, pp 299-318, Springer, Berlin, 2006.

[103] N.A. Murugan, J. Kongsted, Z. Rinkevicius, K. Aidas, K.V. Mikkelsen, H. Ågren, Hybrid density functional theory/molecular mechanics calculations of two-photon absorption of dimethylamino nitro stilbene in solution, Phys. Chem. Chem. Phys. 13 (2011) 12506-12516, DOI: 10.1039/c1cp20611g.

[104] N.A. Murugan, J. Kongsted, Z. Rinkevicius, H. Ågren, Demystifying the solvatochromic reversal in Brooker's merocyanine dye, Phys. Chem. Chem. Phys. 13 (2011) 1290-1292, DOI: 10.1039/c0cp01014f.

[105] S. Forli, R. Huey, M.E. Pique, M.F. Sanner, D.S. Goodsell, A.J. Olson, Computational protein-ligand docking and virtual drug screening with the AutoDock suite, Nat. Protoc. 11(5) (2016) 905-19. DOI: 10.1038/nprot.2016.051.

[106] A. Beheshti, F. Safaeiyan, F. Hashemi, H. Motamedi, P. Mayer, G. Bruno, H. A.Rudbari, Synthesis, structural characterization, antibacterial activity and computational studies of new cobalt (II) complexes with 1,1,3,3-tetrakis (3,5-dimethyl-1-pyrazolyl)propane ligand, J. Mol. Struct. 1123 (2016) 225–237, DOI: 10.1016/j.molstruc.2016.06.037.

[107] E. Kiselev et all, Design, synthesis, pharmacological characterization of a fluorescent agonist of the P2Y14 receptor, Bioorg. Med. Chem. Lett. 25 (2015) 4733–4739, DOI: 10.1016/j.bmcl.2015.08.021.

[108] Ch. Lipinski, F. Lombardo, B.W Dominy, P.J. Feeney, Experimental and computational approaches to estimate solubility and permeability in drug discovery and development setting, Adv. Drug. Deliv. Rev. 23 (1997) 3-25, DOI: 10.1016/S0169-409X(00)00129-0.

[109] J. Manwaring, H. Rothe, C. Obringer, D.J. Foltz, T. R. Baker, J.A. Troutman, N.J. Hewitt, C. Goebel, Extrapolation of systemic bioavailability assessing skin absorption and epidermal and hepatic metabolism of aromatic amine hair dyes in vitro, Toxicol. Appl. Pharmacol. 287(2) (2015) 139-48, DOI: 10.1016/j.taap.2015.05.016.

Graphical abstract

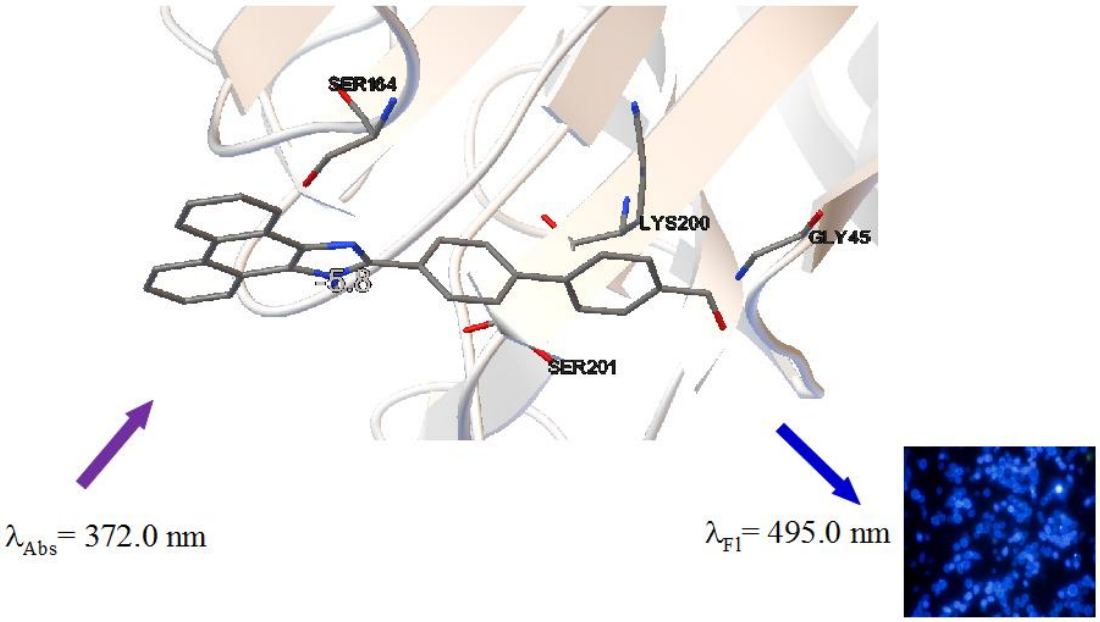

Graphical abstract: Spectroscopic properties of PB2-Concanavalin A conjugate

Figures

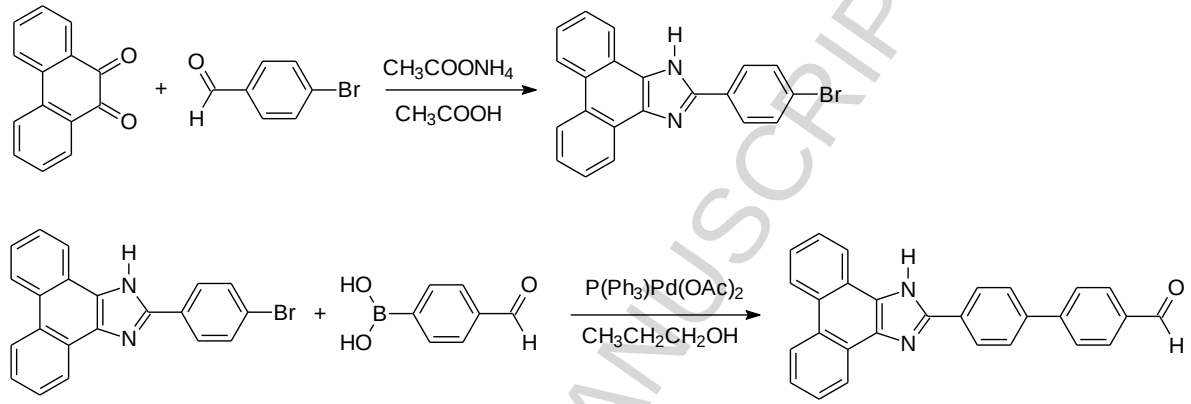

Fig. 1. A route for synthesis of PB2 dye.

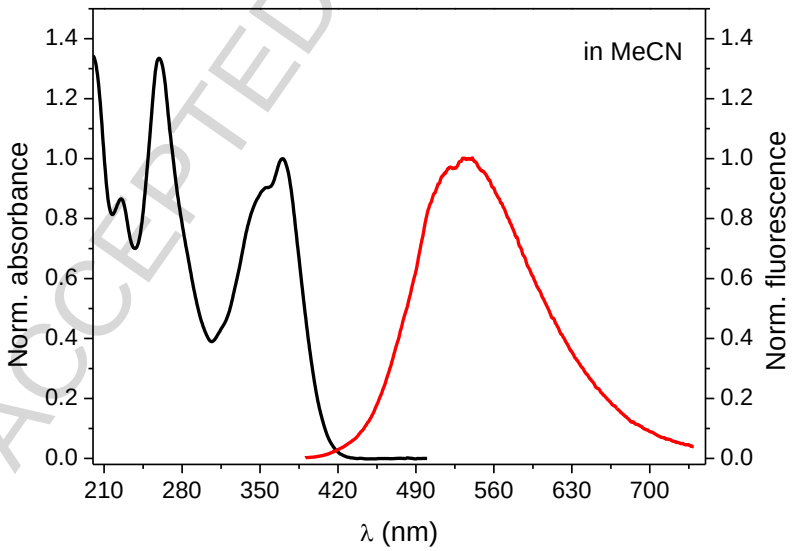

Fig. 2. Normalized electronic absorption and fluorescence spectra of PB2 in MeCN.

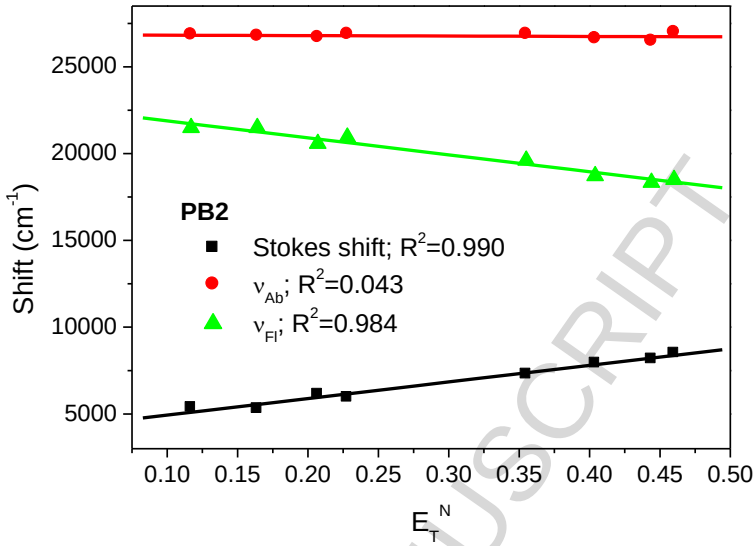

Fig. 3. Influence of solvent polarity on spectral shift for PB2 dye.

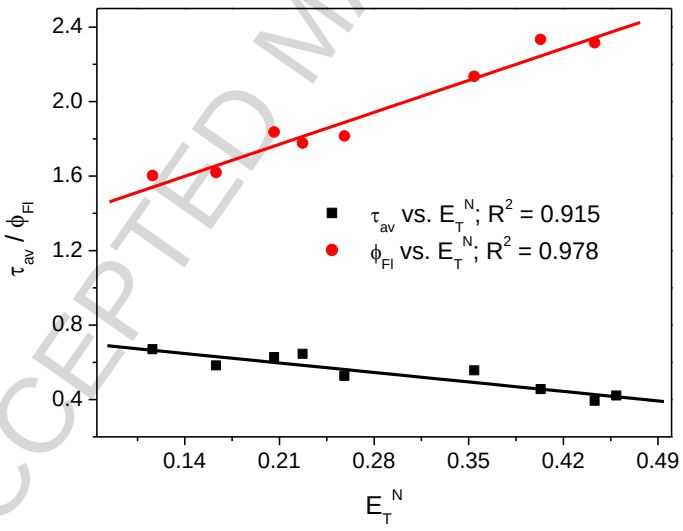

Fig. 4. Plot of both fluorescence quantum yield and averaged fluorescence lifetime of tested compound versus E_T^N.

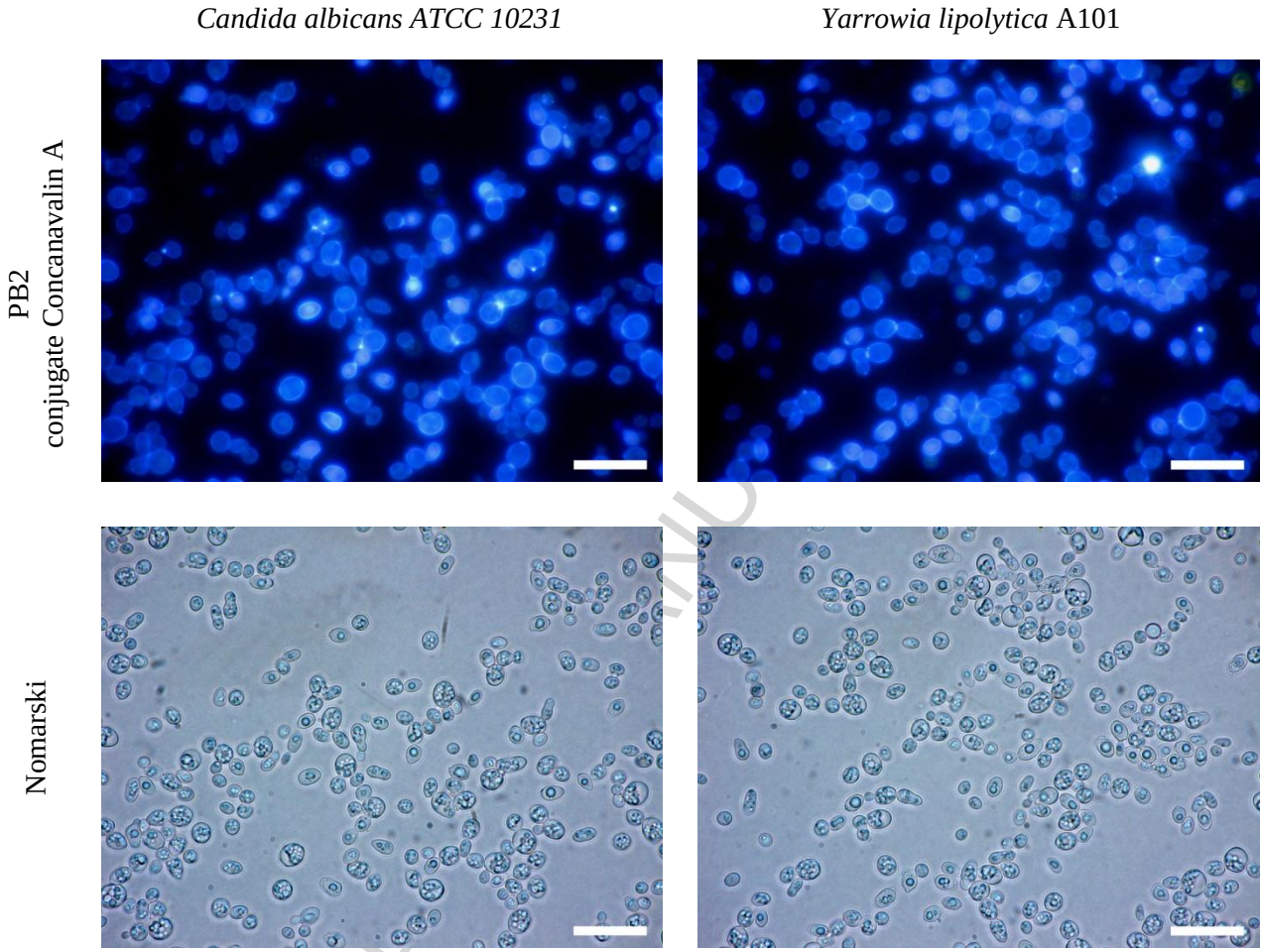

Fig. 5. Fluorescence microscope images of *Candida albicans* and *Yarrowia lipolytica* cells in the presence of dye-protein conjugate. The lectin Concanavalin A labelled with PB2 binds specifically to polysaccharides present in the cell wall of this yeast and fluoresces blue. Scale bars – 20 µm.

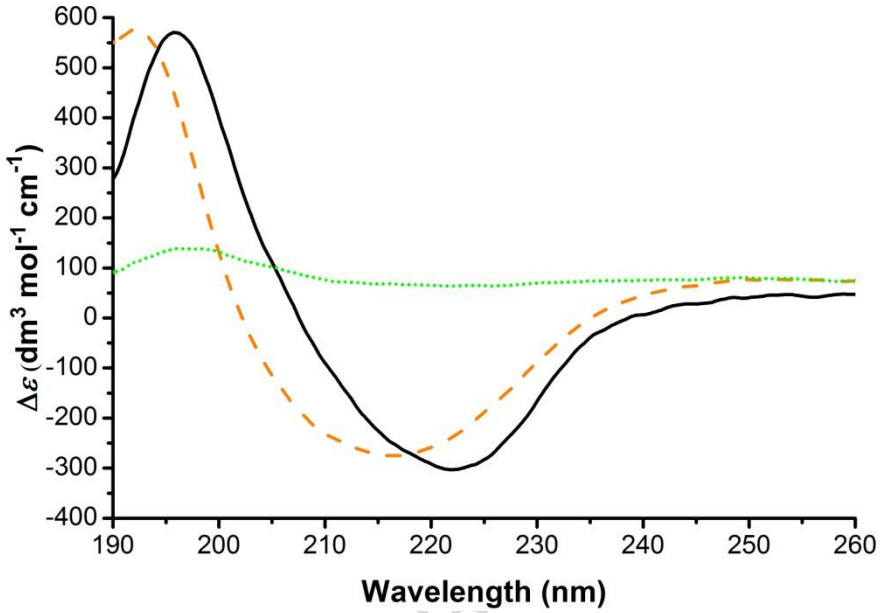

Fig.6. Circular dichroism spectra of Concanavalin A (0.1 mg/mL) in presence of PB2 fluorochrome. Concanavalin A (solid line); PB2-Concanavalin A (dashed line); PB2 (dotted line).

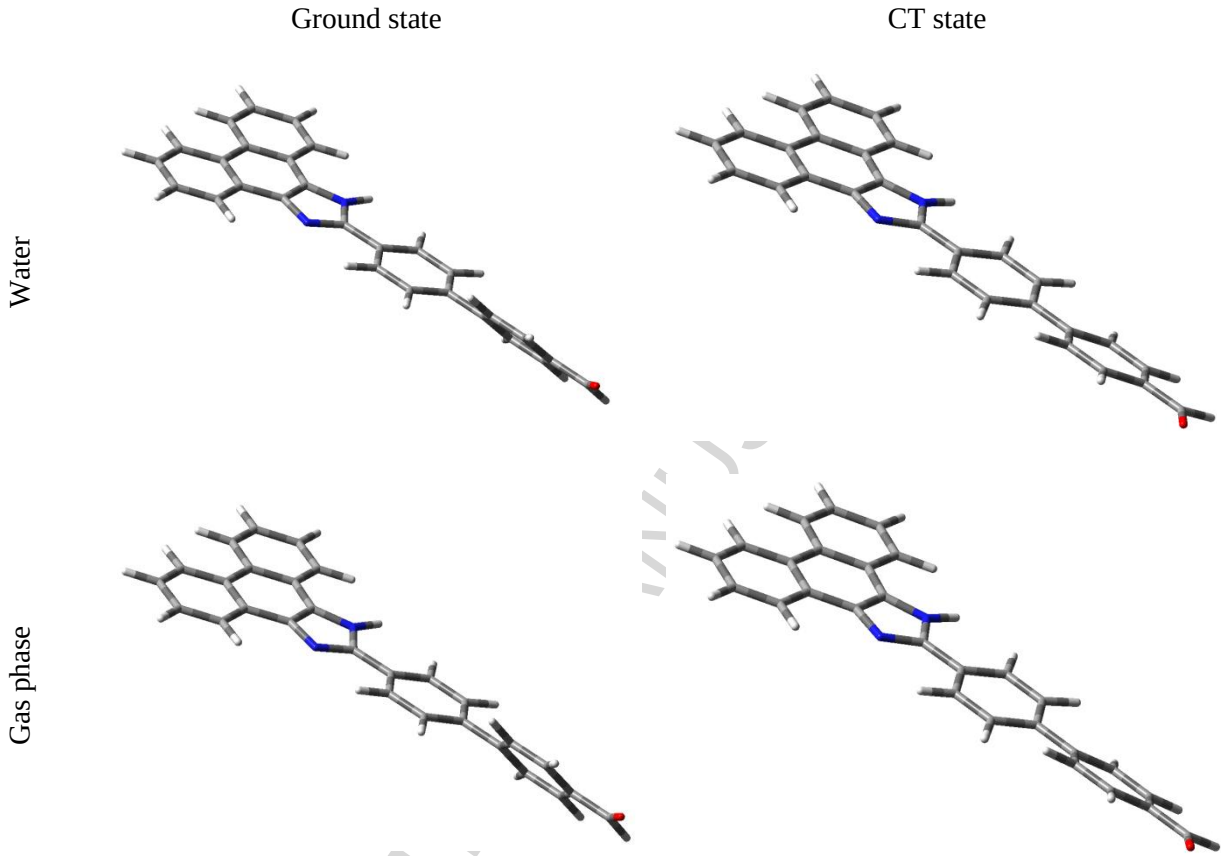

Fig. 7. Structures of studied dye in selected solvents.

LUMO 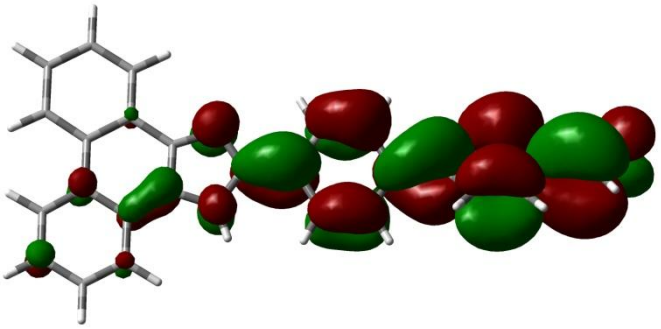 E= -3.5609 eV

HOMO 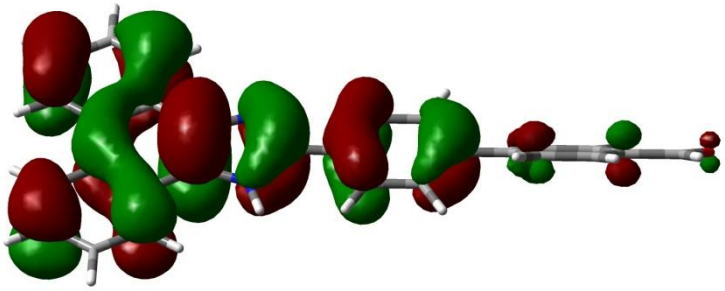 E= -5.514 eV

Fig. 8. Plots of HOMO and LUMO for PB2 dye.

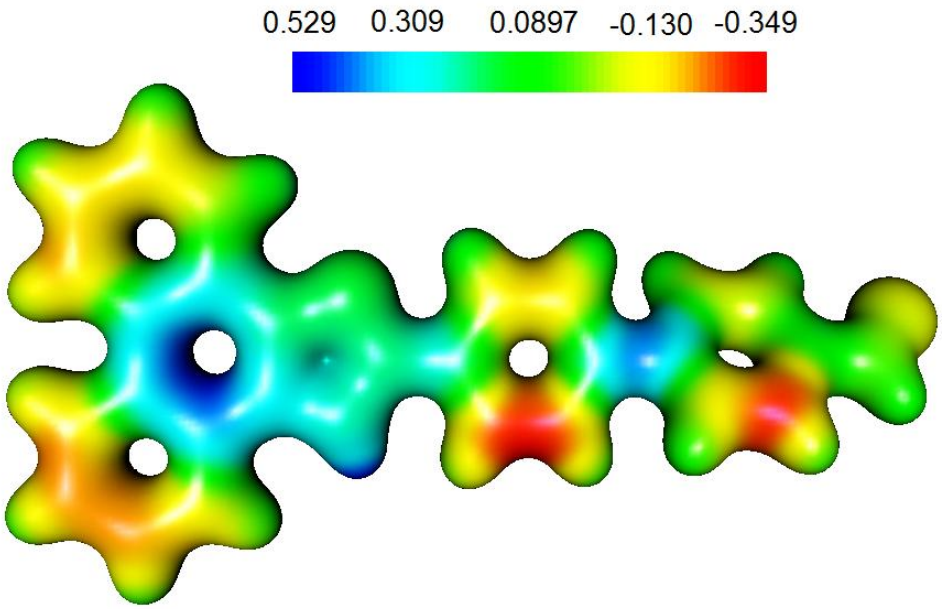

Fig. 9. The MEP surfaces for PB2 dye. Values are expressed in a.u.

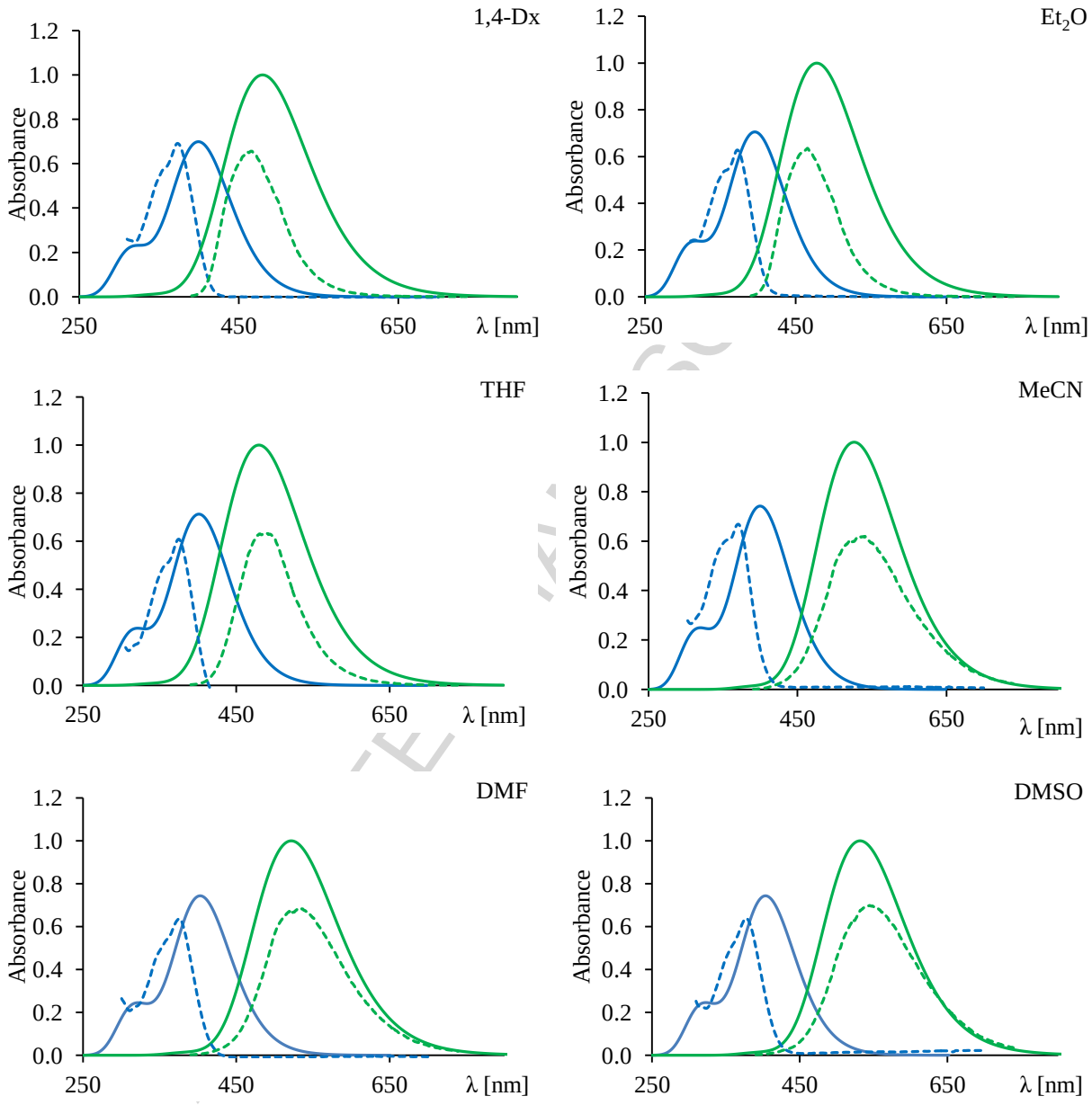

Fig. 10. Comparison of vertical excitation (blue line) and de-excitation (green line) energies designated theoretically (solid line) with measured experimentally (dotted line).

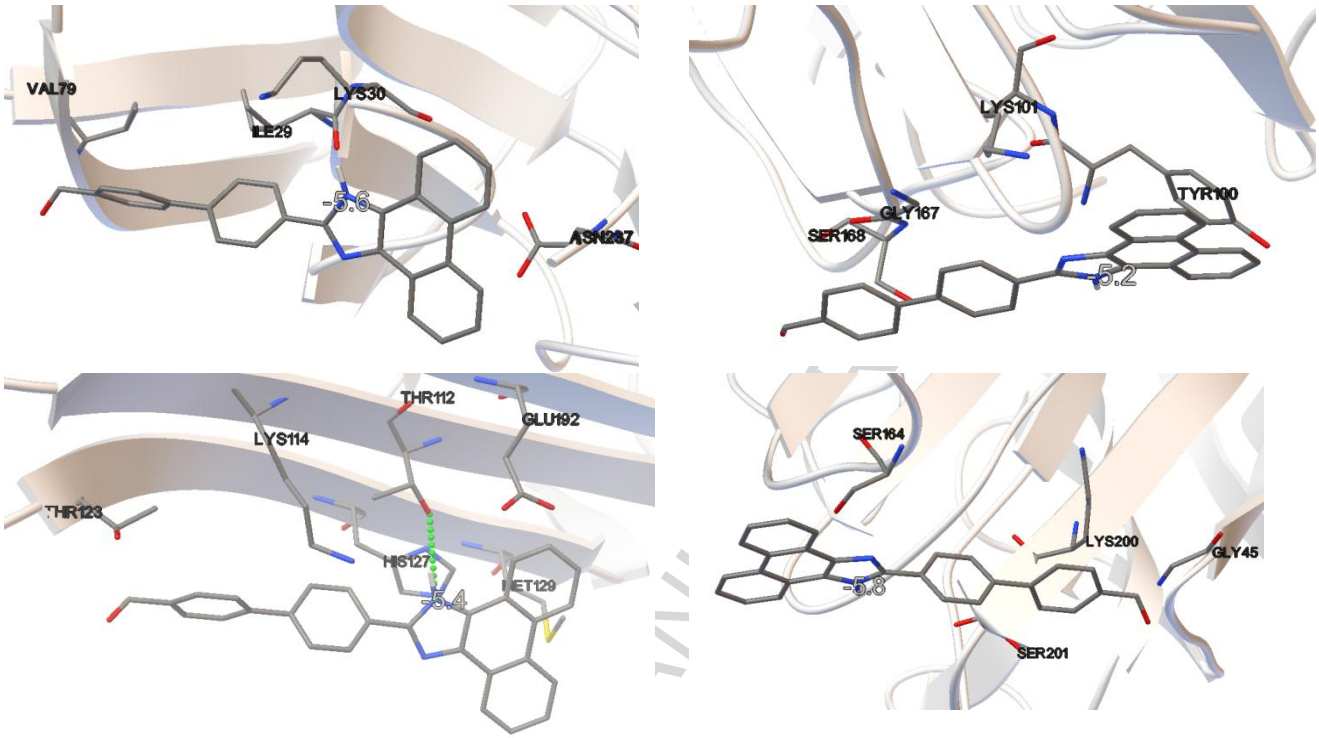

Fig. 11. Interactions between PB2 dye and the active sites in the *Concanavalin A*.

Tables

Table 1. Values of the absorption and fluorescence maximum positions, molar absorption coefficients, Stokes shifts and fluorescence quantum yields for the tested dye.

	λ_{max}^{Ab} [nm]	ε [$M^{-1}cm^{-1}$]	λ_{max}^{Fl} [nm]	ϕ_{Fl} [nm]	$\Delta\nu^{St}$ [cm^{-1}]
1,4-Dx	373.5	44600	465.4	0.577	5287
Et_2O	372.5	36400	465.4	0.664	5359
THF	374.5	39200	486	0.622	6126
MeCN	370.5	37050	540.6	0.416	8493
DMF	375.5	39800	534.2	0.4497	7912
DMSO	377.5	35900	545.4	0.3879	8155

Table 2. Fluorescence lifetimes of PB2 in different solvents.

	τ_1 [ns]	τ_2 [ns]	α_1	α_2	$\tau_{śr}$ [ns]	χ^2
1,4-Dx	0.512	1.843	17.21	82.79	1.614	1.235
Et_2O	0.484	1.675	6.564	93.44	1.597	1.229
THF	0.509	1.963	9.144	90.86	1.830	1.312
MeCN	0.403	1.889	6.28	93.72	1.796	1.212
DMF	0.411	2.438	5.445	94.56	2.328	1.278
DMSO	0.421	2.445	6.657	93.34	2.310	1.304

Table 3. Radiative (k_r) and non-radiative (k_{nr}) rate constants in different solvents.

	k_r (10^8 s^{-1})	k_{nr} (10^8 s^{-1})	k_r / k_{nr}
1,4-Dx	3.58	2.62	0.73
Et_2O	4.16	2.10	0.51
THF	3.40	2.07	0.61
MeCN	2.32	3.25	1.40
DMF	1.93	2.36	1.22
DMSO	1.68	2.65	1.58

Table 4. Calculated free energies of solvation in kcal/mol.

	$\Delta G_{solvation}$		
	CAM-B3LYP	LC-ωPBE	PBE0
1,4-Dx	-20.92	-20.42	-23.40
Et_2O	-21.86	-21.60	-23.62
THF	-22.77	-22.71	-24.72
MeCN	-27.01	-27.84	-26.95
DMF	-24.73	-25.95	-25.14
DMSO	-21.14	-21.33	-22.46
Water	-14.55	-15.65	-14.83

Table 5. The vertical and SS corrected excitation and ed-excitation energies (in nm) and oscillator strength calculated using PBE0.

	TDDFT			cLR-TDDFT	
	λ_{calc}^{Ab}	f_{os}	λ_{calc}^{Fl}	λ_{calc}^{Ab}	λ_{calc}^{Fl}
Gas phase	391.48	0.8306	446.46	---	---
1,4-Dx	399.88	1.0156	479,86	419.99	487.88
Et_2O	396.26	1.0063	478.00	421.43	507.10
THF	401.78	1.0319	479.50	425.12	519.05
MeCN	400.33	1.0230	526.10	418.57	552.96
DMF	403.42	1.0507	521.78	422.39	556.31
DMSO	404.21	1.0472	531.64	422.09	554.42
Water	400.03	1.0208	524.41	418.68	553.21

Highlights

1. For PB2 dye the charge-transfer excited state is more planar than the ground state.

2. The PB2 compound exhibits the non-monotonic solvatochromism.

3. The PB2 dye has potential applicability as a fluorescent probe

4. The PB2 conjugates with Conconavalin A in the active site near LYS200